7080 Inorg. Chem. **2010**, *49*, 7080–7096
DOI: 10.1021/ic1009187

Inorganic Chemistry
Article

Exploring the Effects of H-Bonding in Synthetic Analogues of Nickel Superoxide Dismutase (Ni-SOD): Experimental and Theoretical Implications for Protection of the Ni−SCys Bond

Eric M. Gale, Beulah S. Narendrapurapu, Andrew C. Simmonett, Henry F. Schaefer III, and Todd C. Harrop*

Department of Chemistry and Center for Computational Chemistry, University of Georgia, 1001 Cedar Street, Athens, Georgia 30602

Received May 7, 2010

Nickel superoxide dismutase (Ni-SOD) is a recently discovered SOD obtained from soil microbes and cyanobacteria that shares no structural or spectroscopic similarities with other isoforms of SOD. The enzyme is found in both the Ni^{II} ($Ni\text{-}SOD_{red}$) and Ni^{III} ($Ni\text{-}SOD_{ox}$) oxidation states in "as isolated" preparations of the enzyme from two separate and independently crystallized *Streptomyces* strains. Ni-SOD contains an unusual and unprecedented biological coordination sphere comprised of Cys-S and peptido-N donors. To understand the role of these donors, we have previously synthesized the monomeric $Ni^{II}N_2S_2$ complexes, $(Et_4N)[Ni(nmp)(SC_6H_4\text{-}p\text{-}Cl)]$ (**2**) and $(Et_4N)[Ni(nmp)(S^tBu)]$ (**3**) as $Ni\text{-}SOD_{red}$ models arising from the S,S-bridged precursor molecule, $[Ni_2(nmp)_2]$ (**1**) (where nmp^{2-} = doubly deprotonated form of *N*-2-(mercaptoethyl)picolinamide). In addition to **2** and **3**, we report here three new complexes, $(Et_4N)[Ni(nmp)(S\text{-}o\text{-}babt)]$ (**4**), $(Et_4N)[Ni(nmp)(S\text{-}meb)]$ (**5**), and K[Ni(nmp)(S-NAc)] (**6**) (where $^-$S-*o*-babt = thiolate of *o*-benzoylaminobenzene thiol; $^-$S-meb = thiolate of *N*-(2-mercaptoethyl)benzamide; and $^-$S-NAc = thiolate of *N*-acetyl-L-cysteine methyl ester), that provide a unique comparison as to the structural and reactivity effects imparted by H-bonding in square planar asymmetrically coordinated $Ni^{II}N_2S_2$ complexes. X-ray structural analysis in combination with cyclic voltammetry (CV), spectroscopic measurements, density functional theory (DFT) calculations, and reactivity studies with O_2 and various ROS were employed to gain insight into the role that H-bonding plays in NiN_2S_2 complexes related to Ni-SOD. The experimental results coupled with theoretical analysis demonstrate that H-bonding to coordinated thiolates stabilizes S-based molecular orbitals relative to those arising from Ni^{II}, allowing for enhanced Ni contribution to the highest occupied molecular orbital (HOMO), which is predominantly of S−Ni π^* character. These studies provide a unique perspective on the role played by electronically different thiolates regarding the intimately coupled interplay and delicate balance of Ni- versus S-based reactivity in Ni-SOD model complexes. The reported results have offered new insight into the chemistry that H-bonding/thiolate protonation imparts upon the Ni-SOD active site during catalysis, in particular, as a protective mechanism against oxidative modification/degradation.

Introduction

The superoxide anion radical ($O_2^{\bullet-}$) is an inevitable and cytotoxic byproduct of aerobic metabolism.[1−3] If this reactive oxygen species (ROS) is not eliminated, significant damage to surrounding cells will occur, leading to a variety of disease states.[4] Indeed, the formation of ROS such as superoxide have been implicated in diseases such as diabetes,[2] cancer,[5,6] neurodegenerative disorders like Alzheimer's[3,7] and Parkinson's,[4,8] and the cell death and tissue damage that occurs following stroke or heart attack.[3,9] To combat the adventitious production of this ROS, all aerobes possess metalloenzyme defense systems known as superoxide dismutases (SODs)[4,10] that catalyze the disproportionation of $O_2^{\bullet-}$ to H_2O_2 and O_2 through alternate oxidation and reduction of

---

*To whom correspondence should be addressed. E-mail: tharrop@chem.uga.edu.

(1) Beyer, W.; Imlay, J.; Fridovich, I. *Prog. Nucleic Acid Res. Mol. Biol.* **1991**, *40*, 221.

(2) Maritim, A. C.; Sanders, R. A.; Watkins, J. B., III *J. Biochem. Mol. Toxicol.* **2003**, *17*, 24.

(3) Valentine, J. S.; Wertz, D. L.; Lyons, T. J.; Liou, L.-L.; Goto, J. J.; Gralla, E. B. *Curr. Opin. Chem. Biol.* **1998**, *2*, 253.

(4) Riley, D. P. *Chem. Rev.* **1999**, *99*, 2573.

(5) Kumar, B.; Koul, S.; Khandrika, L.; Meacham, R. B.; Koul, H. K. *Cancer Res.* **2008**, *68*, 1777.

(6) Ishikawa, K.; Takenaga, K.; Akimoto, M.; Koshikawa, N.; Yamaguchi, A.; Imanishi, H.; Nakada, K.; Honma, Y.; Hayashi, J.-I. *Science* **2008**, *320*, 661.

(7) De Leo, M. E.; Borrello, S.; Passantino, M.; Palazzotti, B.; Mordente, A.; Daniele, A.; Filippini, V.; Galeotti, T.; Masullo, C. *Neurosci. Lett.* **1998**, *250*, 173.

(8) Kocatürk, P. A.; Akbostanci, M. C.; Tan, F.; Kavas, G. Ö. *Pathophysiology* **2000**, *7*, 63.

(9) Fortunato, G.; Pastinese, A.; Intrieri, M.; Lofrano, M. M.; Gaeta, G.; Censi, M. B.; Boccalatte, A.; Salvatore, F.; Sacchetti, L. *Clin. Biochem.* **1997**, *30*, 569.

(10) Miller, A.-F. *Curr. Opin. Chem. Biol.* **2004**, *8*, 162.

Scheme 1. Chemistry Catalyzed by SOD Split into Half-Reactions

$$\mathrm{M^{ox}} + \mathrm{O_2^{\bullet-}} \longrightarrow \mathrm{M^{red}} + \mathrm{O_2} \tag{1}$$

$$\mathrm{M^{red}} + \mathrm{O_2^{\bullet-}} + 2\,\mathrm{H^+} \longrightarrow \mathrm{M^{ox}} + \mathrm{H_2O_2} \tag{2}$$

their respective metal centers (eqs 1 and 2, Scheme 1). Several distinct types of SOD are known and each is classified by the first-row transition-metal utilized to carry out the chemistry. The more widely studied SODs include the mononuclear Mn-SOD[11] and Fe-SOD,[12,13] and the dinuclear Cu/Zn-SOD,[14] which have been extensively characterized by numerous biochemical, structural and theoretical studies.

Chart 1. (Top): Active Site of Ni-SOD$_{red}$ (left), Ni-SOD$_{ox}$ (middle), and Ni-SOD Model Systems Described in the Present Work, [Ni(nmp)(SR)]$^-$ (right). (Bottom): R Groups Used in This Study [RSH = HSC$_6$H$_4$-*p*-Cl (**2**), HS^{t}Bu (**3**), *o*-benzoylaminobenzene thiol (**4**), *N*-(2-mercaptoethyl)benzamide (**5**), and *N*-acetyl-L-cysteine methyl ester (**6**)]

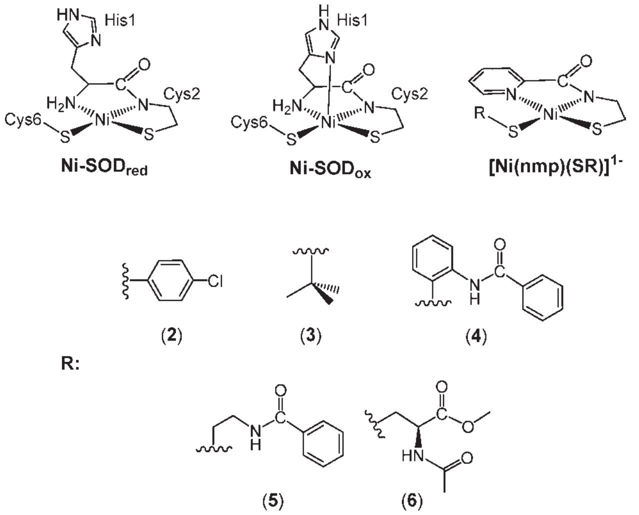

Recently, a distinct class of SOD has been discovered from *Streptomyces* soil microbes and cyanobacteria that contain Ni at the active site.[15−18] These new SODs show no sequence homology with other SODs, have different and unusual primary coordination spheres, and utilize a metal not normally associated with the binding or activation of O_2 (or its derivatives). Structural studies on Ni-SOD reveal a homohexameric protein comprised of four-helix bundle subunits that contain the Ni center.[15] The Ni ion in each subunit is located within a "Ni-hook" binding motif consisting of residues one through nine starting at the N-terminus. The "Ni-hook" motif is disordered in the apo protein and in the reduced resting state (Ni-SOD$_{red}$) houses the Ni^{II} ion in a square planar coordination environment ligated by the thiolates of Cys2 and Cys6 in a cis arrangement. The deprotonated carboxamide from Cys2 and primary amine from His1 complete the N_2S_2 coordination sphere (Chart 1). In the oxidized Ni^{III} form (Ni-SOD$_{ox}$), the geometry changes to square pyramidal via ligation of the imidazole-Nδ side chain of His1 occupying an apical position (Chart 1).[15] The primary coordination sphere of Ni-SOD is distinct from any other metalloenzyme. In fact, there are few known metal sites in biology with an N-terminal amine-N[19] and/or anionic carboxamido-N incorporated within the ligand framework.[20] Additionally, the Ni-SCys bond is a reoccurring theme for redox-active Ni in biology,[21,22] likely present to modulate the redox potential of the Ni ion to facilitate electron transfer under physiological conditions.[23] Ni-SOD, however, reacts with $O_2^{\bullet-}$ at a diffusion controlled rate (10^9 M^{-1} s^{-1}) to form O_2 and H_2O_2.[24] Ni-SOD thus catalyzes the (trans)formation of molecular species typically associated with the oxidative modification of thiolate ligands.[25] This activity is in stark contrast to metalloenzymes with redox active Ni centers ligated by Cys-S, such as acetyl coenzyme A synthase/carbon monoxide dehydrogenase[21] and NiFe hydrogenase,[26] which function under reducing environments. It has also been well documented that coordination of thiolates to square planar Ni^{II} centers markedly enhances their sensitivity to O_2 and ROS, due in part to a destabilization of the thiolate π-orbitals via a repulsive p(π)-d(π) interaction between the S(p) and Ni(d) orbitals.[27,28] It should be of no surprise then that the stated observations have made Ni-SOD an enzyme of particular interest.[29−41]

This novel class of SODs provides the bioinorganic community a new test-system to understand the features required

---

(11) Borgstahl, G. E. O.; Parge, H. E.; Hickey, M. J.; Beyer, W. F., Jr.; Hallewell, R. A.; Tainer, J. A. *Cell* **1992**, *71*, 107.

(12) Miller, A.-F. *Acc. Chem. Res.* **2008**, *41*, 501.

(13) Tierney, D. L.; Fee, J. A.; Ludwig, M. L.; Penner-Hahn, J. E. *Biochemistry* **1995**, *34*, 1661.

(14) Tainer, J. A.; Getzoff, E. D.; Richardson, J. S.; Richardson, D. C. *Nature* **1983**, *306*, 284.

(15) Barondeau, D. P.; Kassmann, C. J.; Bruns, C. K.; Tainer, J. A.; Getzoff, E. D. *Biochemistry* **2004**, *43*, 8038.

(16) Wuerges, J.; Lee, J.-W.; Yim, Y.-I.; Yim, H.-S.; Kang, S.-O.; Carugo, K. D. *Proc. Natl. Acad. Sci. U.S.A.* **2004**, *101*, 8569.

(17) Youn, H.-D.; Kim, E.-J.; Roe, J.-H.; Hah, Y. C.; Kang, S.-O. *Biochem. J.* **1996**, *318*, 889.

(18) Youn, H.-D.; Youn, H.; Lee, J.-W.; Yim, Y.-I.; Lee, J. K.; Hah, Y. C.; Kang, S.-O. *Arch. Biochem. Biophys.* **1996**, *334*, 341.

(19) Lanzilotta, W. N.; Schuller, D. J.; Thorsteinsson, M. V.; Kerby, R. L.; Roberts, G. P.; Poulos, T. L. *Nat. Struct. Biol.* **2000**, *7*, 876.

(20) Harrop, T. C.; Olmstead, M. M.; Mascharak, P. K. *Inorg. Chem.* **2006**, *45*, 3424.

(21) Lindahl, P. A. *Biochemistry* **2002**, *41*, 2097.

(22) Volbeda, A.; Fontecilla-Camps, J. C.; Frey, M. *Curr. Opin. Struct. Biol.* **1996**, *6*, 804.

(23) Krüger, H.-J.; Peng, G.; Holm, R. H. *Inorg. Chem.* **1991**, *30*, 734.

(24) Herbst, R. W.; Guce, A.; Bryngelson, P. A.; Higgins, K. A.; Ryan, K. C.; Cabelli, D. E.; Garman, S. C.; Maroney, M. J. *Biochemistry* **2009**, *48*, 3354.

(25) Mullins, C. S.; Grapperhaus, C. A.; Kozlowski, P. M. *J. Biol. Inorg. Chem.* **2006**, *11*, 617.

(26) Volbeda, A.; Garcin, E.; Piras, C.; de Lacey, A. L.; Fernandez, V. M.; Hatchikian, E. C.; Frey, M.; Fontecilla-Camps, J. C. *J. Am. Chem. Soc.* **1996**, *118*, 12989.

(27) Grapperhaus, C. A.; Darensbourg, M. Y. *Acc. Chem. Res.* **1998**, *31*, 451.

(28) Grapperhaus, C. A.; Mullins, C. S.; Kozlowski, P. M.; Mashuta, M. S. *Inorg. Chem.* **2004**, *43*, 2859.

(29) Fiedler, A. T.; Brunold, T. C. *Inorg. Chem.* **2007**, *46*, 8511.

(30) Fiedler, A. T.; Bryngelson, P. A.; Maroney, M. J.; Brunold, T. C. *J. Am. Chem. Soc.* **2005**, *127*, 5449.

(31) Jenkins, R. M.; Singleton, M. L.; Almaraz, E.; Reibenspies, J. H.; Darensbourg, M. Y. *Inorg. Chem.* **2009**, *48*, 7280.

(32) Neupane, K. P.; Gearty, K.; Francis, A.; Shearer, J. *J. Am. Chem. Soc.* **2007**, *129*, 14605.

(33) Neupane, K. P.; Shearer, J. *Inorg. Chem.* **2006**, *45*, 10552.

(34) Shearer, J.; Dehestani, A.; Abanda, F. *Inorg. Chem.* **2008**, *47*, 2649.

(35) Shearer, J.; Long, L. M. *Inorg. Chem.* **2006**, *45*, 2358.

(36) Shearer, J.; Neupane, K. P.; Callan, P. E. *Inorg. Chem.* **2009**, *48*, 10560.

(37) Shearer, J.; Zhao, N. *Inorg. Chem.* **2006**, *45*, 9637.

(38) Pelmenschikov, V.; Siegbahn, P. E. M. *J. Am. Chem. Soc.* **2006**, *128*, 7466.

(39) Lee, H.-I.; Lee, J.-W.; Yang, T.-C.; Kang, S.-O.; Hoffman, B. M. *J. Biol. Inorg. Chem.* **2010**, *15*, 175.

(40) Ryan, K. C.; Johnson, O. E.; Cabelli, D. E.; Brunold, T. C.; Maroney, M. J. *J. Biol. Inorg. Chem.* **2010**, *15*, 795.

(41) Johnson, O. E.; Ryan, K. C.; Maroney, M. J.; Brunold, T. C. *J. Biol. Inorg. Chem.* **2010**, *15*, 777.

for SOD's crucial biological function in ROS regulation. To date, there is a paucity of information on small-molecule analogues (low MW, non-peptide-based) of Ni-SOD. Recently, a series of peptide-based maquettes consisting of 7 to 12 amino acid residues that are present in the "Ni-hook" region have been synthesized,[32,35,42−44] affording the first examples of functional Ni-SOD analogues. For example, studies by Shearer and co-workers employing $[Ni(SOD^{M2})]$ (where SOD^{M2} = HCDLPCG), which catalytically disproportionates $O_2^{\bullet-}$, provide evidence suggestive of an outer-sphere mechanism for the enzyme.[32] A contradictory study using a similar maquette with the nonapeptide HCDLPCGVY was shown to bind one CN^- at the Ni site supporting an inner-sphere mechanism.[42] It is difficult to delineate the differences between these two very similar systems and the noted differences could be due to the relative instability of some of the maquettes. For example, the nonapeptide Ni-maquette is shown to exist in equilibrium with a 2:1 Ni/peptide and a 1:1 Ni/peptide species in solution.[44] This observation alone warrants the need for more discrete and crystallizable small molecule analogues. One small-molecule analogue directly related to Ni-SOD, namely, $[Ni^{II}(BEAAM)]^-$, has been structurally characterized and consists of an $N_{amine}N_{carboxamide}S_2$ primary coordination sphere.[37] The quasi-reversible $Ni^{III/II}$ couple at 120 mV (vs Ag/AgCl in MeCN) is within the potential window for SOD chemistry, but the complex does not disproportionate $O_2^{\bullet-}$.[45] For all known analogue systems, the Ni^{III} state was transiently observed by EPR in only one case,[32] and all maquette systems were shown to degrade under aerobic conditions. The synthesis and properties of related $Ni^{II}N_3S$[31,46,47] and $Ni^{II}N_2S_2$[48−50] systems have also been reported to replicate some features of the enzyme. At present, however, no model has been studied which incorporates additional second-sphere effects such as hydrogen-bonding (H-bonding). A close inspection of the Ni-SOD active site reveals potential H-bonding interactions between the Cys6-S and the peptide-NH from Val8 and Gly7.[15] An in silico study on $Ni^{II}N_2S_2$ Ni-SOD models demonstrated that the incorporation of one H-bond diminished the reactivity/nucleophilicity of the coordinated-S, placing the greatest electron density at the Ni center, consistent with less S-contribution to the highest occupied molecular orbital (HOMO).[25] However, this effect has yet to be tested experimentally.

Previously, we reported a general methodology toward the preparation of asymmetric square planar $Ni^{II}N_2S_2$ complexes as synthetic analogues of the $Ni\text{-}SOD_{red}$ active site.[51] Addition of *para*-chlorobenzene thiolate ($^-SC_6H_4$-*p*-Cl) or *tert*-butyl thiolate ($^-S^tBu$) to the dinuclear metallosynthon $[Ni_2(nmp)_2]$ (**1**) (where $nmpH_2$ = *N*-2-(mercaptoethyl)picolinamide and Hs represent dissociable protons) resulted in S, S-bridge splitting and the formation of the monomeric complexes, $(Et_4N)[Ni(nmp)(SC_6H_4\text{-}p\text{-}Cl)]$ (**2**) and $(Et_4N)[Ni(nmp)(S^tBu)]$ (**3**) in high yields, respectively. Both complexes conform as good structural analogues with the pyridyl-N, carboxamido-N, and thiolato-S of the nmp^{2-} ligand modeling the contributions of His-1 and Cys-2 in Ni-SOD. The exogenously added thiolate allows for variable (to probe second-sphere effects) and unconstrained modeling of Cys-6 in Ni-SOD utilizing electronically different thiolate ligands. Inspired by the structural and spectroscopic similarities demonstrated by **2** and **3** with $Ni\text{-}SOD_{red}$, namely, their proton accepting capabilities, we set out to synthesize complexes building off of the Ni(nmp) framework with a peptide functionality capable of engaging in H-bonding with the coordinated thiolates. Indeed, results by Solomon et al. suggest that cysteine thiolates may be protonated during catalysis,[52] and theoretical accounts regarding the role played by H-bonding to Ni-coordinated thiolates,[25,53] as well as other metal-bound thiolates in biology,[54−56] have been suggested as mechanisms to protect the CysS donors from oxidative damage. Thus, the objective of the present work was to incorporate key H-bonding functionalities into our model system to gain a fundamental understanding of what electronic properties they impart on the Ni center germane to SOD catalysis. Herein, we present the synthesis, structure, and properties of three new $Ni^{II}N_2S_2$ complexes as part of our $[Ni(nmp)(SR)]^-$ series, namely, $(Et_4N)[Ni(nmp)(S\text{-}o\text{-}babt)]$ (**4**) (HS-*o*-babt = *o*-benzoylaminobenzenethiol), $(Et_4N)[Ni(nmp)(S\text{-}meb)]$ (**5**) (HS-meb = *N*-(2-mercaptoethyl)benzamide), and K[Ni(nmp)(S-NAc)] (**6**) (HS-NAc = *N*-acetyl-L-cysteine methyl ester) (Chart 1).

Experimental Section

General Information. All reagents were purchased from commercial suppliers and used as received unless otherwise noted. Acetonitrile (MeCN), methylene chloride (CH_2Cl_2), tetrahydrofuran (THF), diethyl ether (Et_2O), and pentane were purified by passage through activated alumina columns using an MBraun MB-SPS solvent purification system and stored under a dinitrogen (N_2) atmosphere before use. *N,N*-dimethylformamide (DMF) was purified with a VAC Solvent Purifier containing 4 Å molecular sieves and stored under similar conditions. Triethylamine (TEA) was purified by static drying over Na_2SO_3. All reactions were performed under an inert atmosphere of N_2 using standard Schlenk line techniques or in an MBraun Unilab glovebox under an atmosphere of purified N_2. The molecule, *o*-benzoylaminobenzene thiolate disulfide (disulfide of S-*o*-babt) was synthesized according to a published procedure.[57] The purity was confirmed by comparison with previously reported spectral data. The synthesis

---

(42) Tietze, D.; Breitzke, H.; Imhof, D.; Kothe, E.; Weston, J.; Buntkowsky, G. *Chem.—Eur. J.* **2009**, *15*, 517.

(43) Krause, M. E.; Glass, A. M.; Jackson, T. A.; Laurence, J. S. *Inorg. Chem.* **2010**, *49*, 362.

(44) Schmidt, M.; Zahn, S.; Carella, M.; Ohlenschläger, O.; Görlach, M.; Kothe, E.; Weston, J. *ChemBioChem* **2008**, *9*, 2135.

(45) Tabbì, G.; Driessen, W. L.; Reedijk, J.; Bonomo, R. P.; Veldman, N.; Spek, A. L. *Inorg. Chem.* **1997**, *36*, 1168.

(46) Mullins, C. S.; Grapperhaus, C. A.; Frye, B. C.; Wood, L. H.; Hay, A. J.; Buchanan, R. M.; Mashuta, M. S. *Inorg. Chem.* **2009**, *48*, 9974.

(47) Jenkins, R. M.; Singleton, M. L.; Leamer, L. A.; Reibenspies, J. H.; Darensbourg, M. Y. *Inorg. Chem.* **2010**, *49*, 5503.

(48) Ma, H.; Chattopadhyay, S.; Petersen, J. L.; Jensen, M. P. *Inorg. Chem.* **2008**, *47*, 7966.

(49) Ma, H.; Wang, G.; Yee, G. T.; Petersen, J. L.; Jensen, M. P. *Inorg. Chim. Acta* **2009**, *362*, 4563.

(50) Mathrubootham, V.; Thomas, J.; Staples, R.; McCraken, J.; Shearer, J.; Hegg, E. L. *Inorg. Chem.* **2010**, *49*, 5393.

(51) Gale, E. M.; Patra, A. K.; Harrop, T. C. *Inorg. Chem.* **2009**, *48*, 5620.

(52) Szilagyi, R. K.; Bryngelson, P. A.; Maroney, M. J.; Hedman, B.; Hodgson, K. O.; Solomon, E. I. *J. Am. Chem. Soc.* **2004**, *126*, 3018.

(53) Prabhakar, R.; Morokuma, K.; Musaev, D. G. *J. Comput. Chem.* **2006**, *27*, 1438.

(54) Dey, A.; Jenney, F. E., Jr.; Adams, M. W. W.; Johnson, M. K.; Hodgson, K. O.; Hedman, B.; Solomon, E. I. *J. Am. Chem. Soc.* **2007**, *129*, 12418.

(55) Dey, A.; Okamura, T.; Ueyama, N.; Hedman, B.; Hodgson, K. O.; Solomon, E. I. *J. Am. Chem. Soc.* **2005**, *127*, 12046.

(56) Maynard, A. T.; Covell, D. G. *J. Am. Chem. Soc.* **2001**, *123*, 1047.

(57) Harrop, T. C.; Olmstead, M. M.; Mascharak, P. K. *Chem. Commun.* **2003**, 410.

and characterization of [Ni_2(nmp)$_2$] (**1**), (Et_4N)[Ni(nmp)(SC_6H_4-*p*-Cl)] (**2**), and (Et_4N)[Ni(nmp)(S^{t}Bu)] (**3**) were reported elsewhere.[51]

Physical Methods. FTIR spectra were collected on a Thermo-Nicolet 6700 spectrophotometer running the OMNIC software. Solid-state samples were prepared as pressed KBr pellets, and solution samples were prepared in an airtight Graseby-Specac solution cell with CaF_2 windows and 0.1 mm spacers. Electronic absorption spectra were run at 298 K using a Cary-50 spectrophotometer containing a Quantum Northwest TC 125 temperature control unit. The UV−vis samples were prepared in gastight Teflon-lined screw cap quartz cells equipped with a rubber septum and an optical pathlength of 1 cm. Cyclic voltammetry measurements were performed with a PAR Model 273A potentiostat using a Ag/AgCl reference electrode, Pt counter electrode, and a Glassy Carbon (10 μm diameter) working electrode. Measurements were performed at ambient temperature using 5.0 mM analyte in the appropriate solvent under Ar containing 0.1 M ^{n}Bu$_4$NPF$_6$ as the supporting electrolyte. The "Maximize Stability" mode was utilized in the PAR PowerCV software utilizing a low-pass 5.3 Hz filter. To ensure accuracy in the measured CVs, these experiments were performed in triplicate while polishing the working electrode between each run and report an average E_{ox} in Table 2. Additionally, potentials were checked and corrected by recording the CV of a ferrocene standard under the same experimental conditions as the complexes before each run. NMR spectra were recorded in the listed deuterated solvent on a 400 MHz Bruker BZH 400/52 NMR spectrometer or 500 MHz Varian Unity INOVA NMR spectrometer at ambient temperature with chemical shifts referenced to TMS or residual protio signal of the deuterated solvent. Low resolution electrospray ionization mass spectrometry (ESI-MS) data were collected using a Perkin-Elmer Sciex API I Plus quadrupole mass spectrometer and high resolution ESI-MS data were collected using a Bruker Daltonics 9.4 T APEX Qh FT-ICR-MS. Elemental analysis for C, H, and N was performed at QTI-Intertek in Whitehouse, NJ.

(Et_4N)[Ni(nmp)(S-*o*-babt)] (4). A batch of 81.0 mg (0.177 mmol) of **3** and 44.7 mg (0.0975 mmol) of the disulfide of S-*o*-babt were combined in 10 mL of a 1:1 MeCN/THF mixture at room temperature (RT) to form a red-orange solution. After 16 h of stirring, the reaction mixture was filtered through a 0.2 μm nylon filter, and the mother liquor was concentrated to a red-orange residue. The residue was stirred for 4 h in a mixture of 1:1 THF/Et_2O after which 71.1 mg (0.119 mmol, 67%) of product was isolated as hard red chunks. Dark red blades suitable for X-ray structural analysis were grown by slow diffusion of pentane into a THF solution of **4** at RT. ^{1}H NMR (400 MHz, $CDCl_3$, δ from TMS): 10.57 (s, 1H, NH), 8.47 (d, 1H), 8.32 (m, 4H), 7.76 (m, 2H), 7.48 (m, 4H), 7.19 (t, 1H), 6.99 (t, 1H), 6.84 (t, 1H), 3.45 (t, 2H, OC-NH−C*H*$_2$−CH$_2$−S), 3.11 (q, 8H, (CH$_3$C*H*$_2$)$_4$N), 2.26 (t, 2H, OC-NH−CH$_2$−C*H*$_2$-S), 1.18 (t, 12H, (C*H*$_3$CH$_2$)$_4$N). FTIR (KBr pellet) ν_{max} (cm^{-1}): 3271 (w, NH), 3054 (w), 2979 (w), 2921 (w), 2844 (w), 1652 (s, C=O), 1620 (s, C=O), 1590 (s, C=O), 1574 (s, C=O), 1562 (m), 1525 (m), 1491 (m), 1448 (w), 1428 (m), 1388 (m), 1364 (w), 1331 (w), 1321 (w), 1294 (w), 1254 (w), 1221 (w), 1186 (w), 1171 (w), 1153 (w), 1083 (br, m), 1059 (w), 1031 (w), 997 (m), 942 (w), 896 (w), 813 (w), 786 (w), 768 (m), 761 (s), 715 (w), 686 (w), 669 (w), 623 (w), 587 (w), 557 (w), 542 (w), 484 (w), 463 (w), 449 (w), 432 (w). FTIR (CH_2Cl_2, CaF_2 windows) ν_{max} (cm^{-1}): 3274 (br, w, NH), 3040 (w), 2952 (m), 1670 (m), 1623 (s, C=O), 1600 (s, C=O), 1572 (m), 1521 (s), 1491 (m), 1457 (w), 1429 (m), 1393 (m), 1367 (w). LRMS-ESI (*m*/*z*): [M−Et_4N]$^-$ calcd for $C_{21}H_{18}N_3NiO_2S_2$, 466.0; found, 466.0. UV−vis (MeCN) λ_{max}, nm (ε): 450 (3,500). Anal. Calcd for $C_{29}H_{38}N_4NiO_2S_2\cdot0.5THF\cdot0.5H_2O$: C, 57.95; H, 6.75; N, 8.72. Found: C, 57.63; H, 6.81; N, 8.70.

Synthesis of HS-meb. The synthesis of the ligand comprised the following steps:

Step 1. *N*-(2-(tritylthio)ethyl)benzamide (S-trityl-meb). A batch of 0.975 g (3.05 mmol) of S-trityl-cysteamine and 1.039 g (10.27 mmol) of TEA was dissolved in 10 mL of CH_2Cl_2 and added dropwise over the course of 10 min to a solution of 0.640 g (4.55 mmol) of benzoyl chloride stirring in 2 mL of CH_2Cl_2 at 0 °C. The resulting heterogeneous yellow solution was slowly warmed to RT and stirred for another 48 h before being diluted to homogeneity with CH_2Cl_2 and washed with $NaHCO_3$(aq) and brine. The organic layer was dried over $MgSO_4$, filtered, and concentrated to a yellow oil, which was stirred overnight in a 1:4 mixture of Et_2O/pentane to afford 0.722 g (1.70 mmol, 56%) of product as a fluffy white solid. mp: 125−126 °C. ^{1}H NMR (400 MHz, $CDCl_3$, δ from TMS): 7.71 (m, 2H), 7.51 (m, 2H), 7.43 (m, 8H), 7.26 (t, 6H), 7.21 (t, 3H), 6.25 (br s, 1H, NH), 3.31 (q, 2H, OC-NH−C*H*$_2$−CH$_2$−S), 2.54 (t, 2H, OC-NH−CH$_2$−C*H*$_2$-S). ^{13}C NMR (100.6 MHz, $CDCl_3$, δ from TMS): 167.36 (*C*=O), 144.74, 134.58, 131.60, 129.65, 128.66, 128.13, 127.05, 126.97, 67.03 (*C*Ph$_3$), 45.91 (OC-NH-*C*H$_2$−CH$_2$−S), 32.35 (OC-NH−CH$_2$-*C*H$_2$−S). FTIR (KBr pellet) ν_{max} (cm^{-1}): 3392 (br, m, NH), 3053 (w), 3029 (w), 2930 (w), 1633 (s, C=O), 1601 (w), 1577 (m), 1538 (s), 1488 (m), 1445 (m), 1430 (w), 1361 (w), 1324 (w), 1302 (m), 1235 (w), 1186 (w), 1156 (w), 1077 (w), 1002 (w), 970 (w), 848 (w), 803 (w), 768 (m), 752 (m), 743 (w), 703 (s), 630 (w), 615 (m), 507(w), 474 (w).

Step 2. *N*-(2-mercaptoethyl)benzamide (HS-meb). A batch of 0.533 g (1.26 mmol) of S-trityl-meb was stirred in 10 mL of a 1:1 CH_2Cl_2/TFA solution resulting in a bright yellow solution. After 1 h, 218 mg (1.88 mmol) of Et_3SiH was added dropwise to the solution causing bleaching of the bright yellow solution to a clear and pale yellow color. After 3 h of stirring, the solution was concentrated to ~50% of its original volume, and the resulting insoluble triphenylmethane ($HCPh_3$) byproduct was filtered off and washed with TFA. The solution was then concentrated to a light yellow residue and taken up in 20 mL of CH_2Cl_2 and washed with $NaHCO_3$(aq) and brine. The organic layer was dried over $MgSO_4$, filtered, and concentrated to dryness. The resulting residue was stirred in pentane for 1 h after which 0.218 g (1.20 mmol, 95%) of a white solid product was isolated. mp: 65−66 °C. ^{1}H NMR (400 MHz, $CDCl_3$, δ from TMS): 7.79 (d, 2H), 7.52 (t, 1H), 7.43 (t, 2H), 6.74 (br s, 1H, NH), 3.64 (q, 2H, OC-NH−C*H*$_2$−CH$_2$−S), 2.78 (q, 2H, OC-NH−CH$_2$−C*H*$_2$-S), 1.41 (t, 0.6H, SH, integrates for slightly less because of the exchangeable nature of SH). ^{13}C NMR (100.6 MHz, $CDCl_3$, δ from TMS): 167.66 (*C*=O), 134.46, 131.72, 128.79, 127.07, 42.87 (OC-NH-*C*H$_2$−CH$_2$−S), 24.93 (OC-NH−CH$_2$-*C*H$_2$−S). FTIR (KBr pellet) ν_{max} (cm^{-1}): 3299 (br, m, NH), 3065 (w), 2939 (w), 2840 (w), 2574 (w, SH), 1634 (vs, C=O), 1602 (w), 1579 (m), 1542 (vs), 1491 (m), 1438 (w), 1361 (w), 1310 (s), 1240 (w), 1187 (w), 1155 (w), 1076 (w), 1001 (w), 890 (w), 835 (w), 804 (w), 691 (s), 644 (br, w), 616 (w), 508 (w). FTIR (CH_2Cl_2, CaF_2 windows) ν_{max} (cm^{-1}): 3452 (w, NH), 2977 (w), 2931 (w), 2871 (w), 1665 (s, C=O), 1602 (w), 1581 (w), 1519 (s), 1486 (m), 1414 (w), 1365 (w). LRMS-ESI (*m*/*z*): [M−H]$^-$ calcd for $C_9H_{10}NOS$, 180.1; Found, 180.0.

(Et_4N)[Ni(nmp)(S-meb)] (5). A batch of 68.3 mg (0.149 mmol) of **3** and 32.0 mg (0.177 mmol) of HS-meb were combined in 5 mL of MeCN to afford a red-orange solution. After 16 h of stirring, the reaction mixture was filtered through a 0.2 μm nylon filter, and the mother liquor was concentrated to a red-orange residue. The resulting residue was stirred for 2 h after which 68.4 mg (0.124 mmol, 83%) of red-orange solids were isolated via vacuum filtration. Dark red blades suitable for X-ray crystallography were grown by slow diffusion of Et_2O into a 5:1 THF/DMF solution of **5** at −20 °C. ^{1}H NMR (500 MHz, $CDCl_3$, δ from TMS): 8.51 (br m, 2H, NH and aromatic CH), 8.21 (d, 2H), 7.78 (t, 1H), 7.67 (d, 1H), 7.44 − 7.39 (m, 3H), 7.23 (t, 1H), 3.58 (br, m, 2H), 3.47 (br, t, 2H), 3.40 (q, 8H, (CH$_3$C*H*$_2$)$_4$N), 2.40 (br, s, 2H), 2.31 (br, t, 2H), 1.29 (t, 12H, (C*H*$_3$CH$_2$)$_4$N). FTIR (KBr pellet) ν_{max} (cm^{-1}): 3298 (br, w, NH), 2991 (w), 2932 (w), 2917 (w), 2842 (w), 1643 (s, C=O), 1623 (s, C=O), 1598 (s, C=O), 1575 (w), 1563 (w), 1522 (m), 1485 (m), 1441 (m), 1395 (m), 1296 (m), 1279 (w), 1259 (w), 1185 (w), 1171 (w), 1140 (w), 1084 (m), 1049 (w), 999 (w), 808 (w), 784 (w), 759 (w), 715 (m), 694 (w), 687 (w), 557 (w), 485 (w). FTIR (CH_2Cl_2, CaF_2 windows) ν_{max} (cm^{-1}): 3261 (br, w, NH), 3041 (w), 2962 (w), 2843 (w), 1647 (m, C=O), 1619 (s, C=O), 1598 (s, C=O), 1578 (w), 1563 (w), 1533 (w), 1484 (m), 1458 (w), 1393 (m). LRMS-ESI (*m*/*z*): $[M-Et_4N]^-$ calcd for $C_{17}H_{18}N_3NiO_2S_2$, 418.0; Found, 418.0. UV−vis (MeCN) λ_{max}, nm (ε): 449 (3900). Anal. Calcd for $C_{25}H_{38}N_4NiO_2S_2\cdot 1.25H_2O$: C, 52.50; H, 7.14; N, 9.80. Found: C, 52.51; H, 7.02; N, 9.82.

K[Ni(nmp)(S-NAc)] (6). To a batch of 159.9 mg (0.4355 mmol) of the K^+ salt of **3** in 10 mL of MeCN was added 82.3 mg (0.464 mmol) of *N*-acetyl-L-cysteine methyl ester in 3 mL of MeCN at RT. Upon addition, the reaction mixture rapidly changed from red-orange to a brown-tinged orange solution. After 16 h of stirring, the reaction mixture was filtered through a 0.2 μm nylon filter, and the mother liquor was concentrated to a red-orange residue. Stirring the residue in 1:1 THF/Et_2O afforded free-flowing red-brown solids of which 163.0 mg (0.3588 mmol, 82%) were isolated via vacuum filtration. ^1H NMR (500 MHz, d_6-acetone, δ from protio solvent): 8.73 (s, 0.3 H, NH, integrates for slightly less because of the exchangeable nature of NH), 8.50 (d, 1H), 7.89 (t, 1H), 7.55 (d, 1H), 7.35 (t, 1H), 4.18 (t, 1H, S_{cys}-CH_2−C*H*-), 3.59 (s, 3H, C*H*$_3$-O−CO), 3.36 (m, 1H, S_{nmp}-CH_2−C(*H*)(*H*)-N-CO), 3.32 (m, 1H, S_{nmp}-CH_2−C(*H*)(*H*)-N-CO), 2.29 (m, 3H, S_{cys}-C*H*$_2$-CH- and S_{nmp}-C(*H*)(*H*)-CH_2−N-CO), 2.17 (m, 1H, S_{nmp}-C(*H*)(*H*)-CH_2−N-CO), 2.02 (s, 3H, C*H*$_3$-NH−CO). FTIR (KBr pellet) ν_{max} (cm^{-1}): 3246 (br, w, NH), 2916 (w), 2841 (w), 1735 (m, C=O ester), 1662 (s, C=O), 1620 (s, C=O carboxamide), 1595 (s, C=O), 1562 (m), 1533 (br, m), 1435 (w), 1398 (m), 1373 (m), 1292 (w), 1261 (w), 1214 (w), 1129 (m), 1078 (m), 1005 (w), 761 (w), 687 (w), 633 (w), 625 (w), 560 (w), 487 (w). FTIR (MeCN, CaF_2 windows) ν_{max} (cm^{-1}): 3481 (br, w, NH), 3372 (br, w, NH), 3235 (br, w, NH), 2987 (m), 2937 (m), 2845 (w), 1747 (m, C=O ester), 1671 (s, C=O), 1623 (s, C=O carboxamide), 1600 (s, C=O), 1539 (w). LRMS-ESI (*m*/*z*): $[M-K]^-$ calcd for $C_{14}H_{18}N_3NiO_4S_2$, 414.0; Found, 414.0. HRMS-ESI (*m*/*z*): $[M-K]^-$ calcd for $C_{14}H_{18}N_3NiO_4S_2$ (relative abundance), 414.0092 (100.0), 415.0113 (18.2), 416.0046 (49.9), 417.0067 (10.5), 418.0021 (10.5); Found, 414.0099 (100.0), 415.0137 (14.1), 416.0052 (47.1), 417.0084 (7.0), 418.0022 (8.0). UV−vis (MeCN) λ_{max}, nm (ε): 442 (3,710). Anal. Calcd for $C_{14}H_{18}KN_3NiO_4S_2\cdot 3H_2O$: C, 33.08; H, 4.76; N, 8.27. Found: C, 33.54; H, 4.13; N, 7.83.

Reactivity Studies with O_2 and ROS. All measurements were carried out in gastight Teflon-lined screw cap quartz UV−vis cells of 1 cm pathlength equipped with a rubber septum. All samples were prepared under an anaerobic atmosphere in a glovebox prior to addition of oxidants. The kinetic data were obtained by monitoring the decay of λ_{max} for each Ni complex with respect to time at 298 K. The average rate constants (k_{obs}) along with their standard deviations were calculated from triplicate runs under identical experimental conditions. An absorbance versus time plot was generated in the Cary 50 Scanning Kinetics program, and the data was fit according to the equation $y = (A_0 - A_\infty)e^{-kt} + A_\infty$ where y is the absorbance at λ_{max}, A_0 is the absorbance at time = 0, A_∞ is the absorbance when the oxidation reaction is over, t is time (s), and k (or k_{obs}) is the observed pseudo first-order rate constant.

O_2 Reactions. After the initial spectrum of a 0.13 mM MeCN solution (3.00 mL total volume) of each Ni complex (**2**−**6**) was recorded, dry O_2 gas (via passage through a Drierite column) was bubbled through the septum and into the solution through a long stainless steel syringe needle for 60 s. Assuming saturation, this would afford ~60 mol-equiv O_2 with respect to complex (O_2 solubility in MeCN at 298 K: 8.1 ± 0.6 mM).[58] The UV−vis spectra were then recorded every 15 min for a total time of 4 h under an atmosphere of O_2. FTIR data were obtained via evaporation of reaction solvent to dryness (after 4 h for **3**, **5**, and **6**; 18 h for **4** and **6**), addition of KBr and fresh MeCN and re-evaporation; suitable pellets were pressed from the dried mixture of products and KBr.

H_2O_2 Reactions. After the initial spectrum of a 0.13 mM MeCN solution (3.00 mL total volume) of each Ni complex (**2**−**6**) was recorded, addition of a 0.100 mL aliquot of an MeCN solution of $H_2O_2\cdot$urea (81.0 mM, 20 mol-equiv) was added through the septum via syringe needle. The solution was mixed immediately and the resulting UV−vis spectra were recorded every 12 s for 5 min. An identical procedure was performed employing 50% by wt. H_2O_2(aq), and an analogous decay profile was observed with comparable kinetics. No significant changes in the UV−vis spectrum were observed after adding 20 mol-equiv urea to an MeCN solution of the Ni complexes (**2**−**6**). FTIR data were recorded in a similar fashion to the O_2(g) experiments (H_2O_2(aq) was used since urea would swamp out the FTIR signals from the complex, as a result of degradation of the complex due to the presence of H_2O occurs and results in an intense ν_{CO} peak in the carbonyl region because of the protonated nmpH_2 ligand).

KO_2 Reactions. After the initial spectrum of a 0.13 mM MeCN solution (3.00 mL total volume) of each Ni complex (**2**−**6**) was recorded, a 0.020 mL aliquot of a THF solution (solubilized with 18-crown-6) of KO_2 (29.7 mM, 12 mol-equiv) was added, and the UV−vis spectrum monitored. The same procedure was utilized in the presence of excess imidazole (10 mol-equiv) added to the solution for complexes **4** and **5**.

X-ray Data Collection and Structure Solution Refinement. Suitable crystals were mounted and sealed inside a glass capillary. All geometric and intensity data were measured at 293 K on a Bruker SMART APEX II CCD X-ray diffractometer system equipped with graphite-monochromatic Mo Kα radiation (λ = 0.71073 Å) with increasing ω (width 0.5° per frame) at a scan speed of 10 s/frame or 15 s/frame controlled by the SMART software package.[59] The intensity data were corrected for Lorentz-polarization effects and for absorption[60] and integrated with the SAINT software. Empirical absorption corrections were applied to structures using the SADABS program.[61] The structures were solved by direct methods with refinement by full-matrix least-squares based on F^2 using the SHELXTL-97 software[62] incorporated in the SHELXTL 6.1 software package.[63] The hydrogen atoms were fixed in their calculated positions and refined using a riding model. All non-hydrogen atoms were refined anisotropically. Perspective views of the complexes were obtained using ORTEP.[64] Crystallographic properties are reported in the Supporting Information, Table S1.

Electronic Structure Computations. Supporting theoretical studies were performed by optimizing the geometries of **2**−**6** using density functional theory (DFT). The OPTX pure exchange functional of Handy and Cohen[65] was used in conjunction with the Lee−Yang−Parr correlation functional;[66] this method is commonly denoted as OLYP. To correctly describe the more diffuse regions of the charge density within each molecule, where the negative charge resides, the large def2-TZVPP basis set[67] was used. In addition to geometry optimizations, the atomic charges and the contributions from each atom to the highest occupied molecular orbital (HOMO) were computed. The geometry optimizations

---

(58) Achord, J. M.; Hussey, C. L. *Anal. Chem.* **1980**, *52*, 601.

(59) *SMART: Software for the CCD Detector System*, v5.626; Bruker AXS: Madison, WI, 2000.

(60) Walker, N.; Stuart, D. *Acta Crystallogr.* **1983**, *A39*, 158.

(61) Sheldrick, G. M. *SADABS: Area Detector Absorption Correction*; University of Göttingen: Göttingen, Germany, 2001.

(62) Sheldrick, G. M. *Program for Refinement of Crystal Structures*; University of Göttingen: Göttingen, Germany, 1997.

(63) Sheldrick, G. M. *SHELXTL 6.1, Crystallographic Computing System*; Siemens Analytical X Ray Instruments: Madison, WI, 2000.

(64) Johnson, C. K. *ORTEP-III*, Report ORNL-5138; Oak Ridge National Laboratory: Oak Ridge, TN, 1976.

(65) Cohen, A. J.; Handy, N. C. *Mol. Phys.* **2001**, *99*, 607.

(66) Lee, C.; Yang, W.; Parr, R. G. *Phys. Rev. B* **1988**, *37*, 785.

(67) Weigend, F.; Ahlrichs, R. *Phys. Chem. Chem. Phys.* **2005**, *7*, 3297.

were performed using the QChem3.2[68] package, which also provided atomic charges via its implementation of the natural bond orbital theory software NBO 5.0.[69] The ORCA[70] program was used to obtain orbital compositions within the Löwdin and Mulliken population analysis (MPA) definitions, which yielded essentially identical compositions; for this reason only the Löwdin compositions are reported. Electrostatic potentials were also computed with the ORCA package.

Results and Discussion

Synthesis. The long-term goal of this research is to design and synthesize structural and ultimately functional models of the NiN_2S_2 active site in Ni-SOD. As a step toward this goal, we have employed a ligand with a diverse array of donor centers to replicate the asymmetric nature of the N_2S_2 donor set, for example, amine-N, carboxamido-N, and thiolato-S in the present work. In fact, models employing electronically accurate and spatially disposed N_2S_2 ligand sets in Ni-SOD models are quite rare in the literature.[37,50] For our initial approach at Ni-SOD modeling we have employed the nmp^{2-} N_2S ligand platform, which contains three of the Ni-SOD donors leaving the fourth position amenable to synthetic tuning. Reaction of $[Ni(H_2O)_6](ClO_4)_2$ with nmp^{2-} (deprotonated with 2 mol-equiv of NaH) in a polar aprotic solvent like DMF readily afforded the orange complex, $[Ni_2(nmp)_2]$ (**1**), in quantitative yield.[51] This Ni complex has limited solubility in most common organic solvents and is inherently stable in the solid-state owing to the presumed kinetic inertness of square planar $Ni^{II} = d^8$ and formation of the S, S-bridge imparting O_2 insensitivity. Despite the unfavorable solubility properties of **1**, we proposed that it could serve as a viable metallosynthon for generating monomeric NiN_2S_2 complexes through cleavage of the S,S-bridge in the presence of thiolates. In fact, very recent examples of such $Ni_2(\mu\text{-}SR)_2$ bridge-cleaving reactions with imidazole and thiocarboxylate ligands have been nicely demonstrated by both Darensbourg[31] and Holm,[71] respectively. As reported by us in communication form, the synthesis of the monomeric Ni^{II} complexes **2** and **3** involve the general procedure of cleaving the S,S-bridge of metallosynthon **1** in the presence of two mol-equivs of an exogenously added thiolate (Scheme 2).[51] These complexes were isolated in ~70% yield and have been structurally and spectroscopically characterized (vide infra). Thus, the common notion that $Ni_2(\mu\text{-}SR)_2$ dimers are stable and inert toward bridge-cleavage is incorrect in this case perhaps due to the labilizing effect of the strong-field carboxamido-N that is *trans* to the S-donor in **1**. Collectively, this synthetic route appears to be general for the synthesis of these types of Ni^{II} complexes.

In the present account, we have used the common metallosynthon **1** along with alternative synthetic methodologies to expand the toolbox of routes now available toward monomeric and asymmetric Ni-SOD analogues.

Scheme 2. Synthetic Protocols by Which Complexes of General Formula $[Ni(nmp)(SR)]^-$ Were Obtained

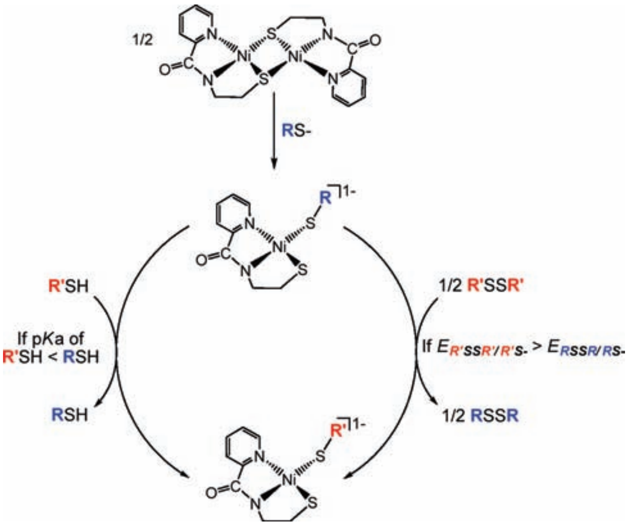

For example, complexes **4**−**6** were synthesized in pure form and in 67−83% yields from monomeric **3** via two chemically distinct paths (Scheme 2). Addition of 0.5 mol-equiv of *o*-benzoylaminobenzene disulfide to **3** rapidly changed the reaction mixture resulting in a subtle dulling of the initial dark red-orange color of **3** to one that is more orange and consistent with formation of **4** (Scheme 2, right-side). A detailed product analysis reveals the disulfide ^{t}BuS−S^{t}Bu, as the only identifiable product formed in this reaction. Analogous disulfide/coordinated-thiolate exchange procedures have been employed previously by Ueyama et al. in the synthesis of [Fe−S] cluster biomimetics,[72] and a similar method has been demonstrated by Holm et al. in the synthesis of the selenolate cluster, $[Fe_4S_4(SePh)_4]^{2-}$, from reaction of PhSe−SePh and $[Fe_4S_4(SPh)_4]^{2-}$ with concomitant formation of PhS−SPh.[73] The aforementioned disulfide exchange reactions are redox-driven and have been attributed to nucleophilic attack of the metal-coordinated thiolate on the more electropositive disulfide bond, resulting in disulfide cleavage and ligand substitution by the more weakly donating thiolate ligand.[72] Studies by Riordan on the disulfide exchange with Ni−CH_3 complexes to form new complexes with a Ni−SR bond and ethane also support a similar mechanism.[74] The obvious advantage of this route is the use of the easily isolable and more stable disulfide versus their corresponding thiols. In fact, many organic sulfur-containing molecules employ protection of the S-moiety as a disulfide to perform further chemical modifications on the molecule that thiol-SH groups would be sensitive to.[75] Thus, one can envision employing this preparation for more complex thiol systems containing other functionalities in the synthesis of a variety of Ni-SOD model systems.

---

[68] Shao, Y.; Molnar, L. F.; Jung, Y.; et al. *Phys. Chem. Chem. Phys.* **2006**, *8*, 3172.

[69] Li, Y.; Zamble, D. B. *Chem. Rev.* **2009**, *109*, 4617.

[70] Neese, F. *ORCA - an ab intio, Density Functional and Semiempirical Program Package*, version 2.7; University of Bonn: Bonn, Germany, 2009.

[71] Huang, D.; Deng, L.; Sun, J.; Holm, R. H. *Inorg. Chem.* **2009**, *48*, 6159.

[72] Ueyama, N.; Yamada, Y.; Okamura, T.; Kimura, S.; Nakamura, A. *Inorg. Chem.* **1996**, *35*, 6473.

[73] Que, L., Jr.; Bobrik, M. A.; Ibers, J. A.; Holm, R. H. *J. Am. Chem. Soc.* **1974**, *96*, 4168.

[74] Ariyananda, P. W. G.; Kieber-Emmons, M. T.; Yap, G. P. A.; Riordan, C. G. *Dalton Trans.* **2009**, 4359.

[75] Greene, T. W.; Wuts, P. G. M. *Protective Groups in Organic Synthesis*; Wiley: New York, 1999.

Table 1. Selected Bond Distances [Å] and Bond Angles [deg] for $(Et_4N)[Ni(nmp)(SC_6H_4\text{-}p\text{-}Cl)]$ (**2**), $(Et_4N)[Ni(nmp)(S^tBu)]$ (**3**), $(Et_4N)[Ni(nmp)(S\text{-}o\text{-}babt)]$ (**4**), $(Et_4N)[Ni(nmp)(S\text{-}meb)]$ (**5**), and Ni-SOD_{red}[15] [a]

	2	**3**	**4**	**5**	**Ni-SOD$_{red}$**
Ni(1)−N(1)	1.8638(14)	1.882(2)	1.877(3)	1.863(7)	1.91(3)
Ni(1)−N(2)	1.9470(14)	1.9635(19)	1.947(3)	1.944(7)	1.87(6)
Ni(1)−S(1)	2.1492(5)	2.1629(7)	2.1518(12)	2.156(3)	2.19(2)
Ni(1)−S(2)	2.2139(4)	2.1938(7)	2.1939(14)	2.172(3)	2.16(2)
N(1)−Ni(1)−N(2)	83.25(6)	82.30(8)	83.77(13)	83.3(3)	83.6(1.6)
N(1)−Ni(1)−S(1)	88.31(5)	87.41(6)	87.67(10)	88.0(2)	88.2(7)
N(1)−Ni(1)−S(2)	176.73(5)	174.21(6)	175.92(10)	175.3(2)	
N(2)−Ni(1)−S(1)	170.64(4)	169.41(6)	171.43(9)	171.3(3)	
N(2)−Ni(1)−S(2)	98.18(4)	92.07(6)	92.16(10)	92.3(3)	93.3(1.3)
S(1)−Ni(1)−S(2)	90.45(2)	98.14(3)	96.40(5)	96.42(11)	95.0(6)
Ni(1)−S(1)−C(1)	99.07(8)	98.42(9)	99.22(16)	98.3(3)	
Ni(1)−S(2)−C(9)	103.32(6)	119.54(8)	115.21(12)	112.2(3)	

[a] In Ni-SOD_{red}: N(1), N(2), S(1), and S(2) correspond to the terminal amine of His1, the amide of Cys2, the thiolate of Cys2, and the thiolate of Cys6, respectively; PDB code 1T6U.

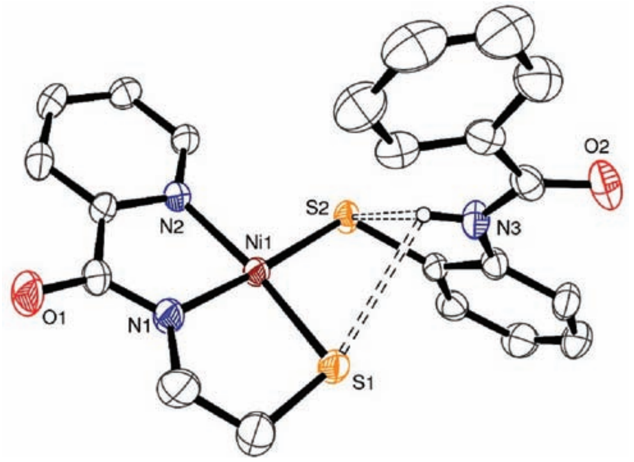

Figure 1. ORTEP diagram of the anion of $(Et_4N)[Ni(nmp)(S\text{-}o\text{-}babt)]$ (**4**) showing 30% thermal ellipsoids for all non-hydrogen atoms. Hydrogen atoms are omitted for clarity with the exception of that attached to N3 to exemplify the presence of intramolecular H-bonding.

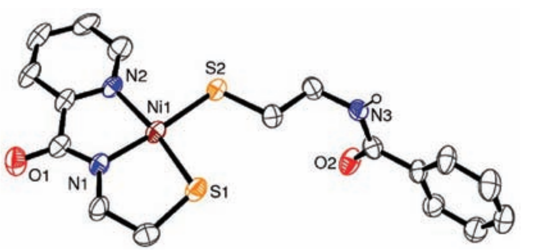

Figure 2. ORTEP diagram of the anion of $(Et_4N)[Ni(nmp)(S\text{-}meb)]$ (**5**) showing 30% thermal ellipsoids for all non-hydrogen atoms. Hydrogen atoms are omitted for clarity with the exception of that attached to N3.

Another route employed a pK_a-driven thiol/coordinated-thiolate ligand exchange reaction (Scheme 2, left-side). Previously, we have demonstrated in systems with the general formula $(Et_4N)[Ni(nmp)(SR)]$, that the monodentate RS^- could be exchanged for a more acidic thiol, namely, generation of **2** and ^{t}BuSH occurs via addition of 1 mol-equiv of the more acidic 4-chlorobenzenethiol to **3** (Scheme 2).[51] In the present work, complexes **5**−**6** were obtained in analytically pure form via an identical procedure. For example, addition of 1 mol-equiv of HS-meb or HS-NAc to an MeCN solution of **3** resulted in rapid and clean formation of **5**−**6**, respectively, as evidenced by spectroscopic methods and/or X-ray crystallography (vide infra). The yields of these reactions are all high ranging from 67% for **4** to 83% for **5**. It is evident that one could employ multiple routes for the synthesis of the Ni-SOD analogues reported in this work. The best route will often be dictated by some physical parameter such as pK_a, the disulfide/thiolate redox potential, and/or the overall synthetic availability of the exogenous thiolate. Regardless of what route is chosen, a large library of NiN_2S_2 complexes analogous to **2**−**6** can be envisioned and synthesized from one common precursor, namely, **1**.

Structural Characterization. Complexes **4**−**5** have been structurally characterized by single crystal X-ray diffraction and, together with the previously reported complexes **2** and **3**,[51] provide a detailed analysis as to the effects imparted on the NiN_2S_2 core of $[Ni(nmp)(SR)]^-$ complexes via modification of the exogenously added thiolate ligand (hereafter S_{exo}). Crystallographic data are given in the Supporting Information, Table S1, and selected bond angles and distances are summarized in Table 1. The molecular structures of **2**−**3** are reported elsewhere[51] and **4**−**5** are shown in Figures 1−2. Not surprisingly, the NiN_2S_2 coordination geometry remains distorted square planar around the Ni^{II} center in all the complexes with little deviation from the least-squares plane defined by the donor atoms (see the Supporting Information, Figures S1−S2). The metric parameters of the Ni(nmp) fragment remain relatively constant with the asymmetric coordination sphere arising in part from the electronically different Ni−N interactions. The $Ni-N_{carboxamide}$ distance (avg: 1.871 Å) is consistently shorter than the $Ni-N_{py}$ (avg: 1.950 Å) because of the strong σ-donating character of this ligand. Structurally similar $Ni^{II}-N_2S_2$ complexes with mixed amine/carboxamide,[37,50] diamine,[28,76] or dicarboxamide[23,77] N-donors have also attributed this shorter distance to the increased ligand-field of the deprotonated carboxamido-N group.[37] The average Ni−S distance (2.155 Å) from the nmp^{2-} ligand (hereafter S_{nmp}) compares well with other $Ni^{II}-SR$ complexes.[23,37,76] Both the $Ni-N_{carboxamide}$ and $Ni-S_{nmp}$ bonds vary by no more than 0.019 Å each, with the longest and shortest $Ni-N_{carboxamide}$ bonds belonging to **3** (1.882(2) Å) and **5** (1.863(7) Å), respectively, apparently due to the trans-influence of the electronically variant S_{exo} ligands (vide infra). The bond angles within the nmp fragment deviate slightly from an ideal square planar polyhedron and remain similar in all complexes; avg. $N_{carboxamide}-Ni-N_{py}$ angle: 83.2°; avg. $S_{nmp}-Ni-N_{carboxamide}$ angle: 87.8° (Table 1). Both of these angles remain acute due to the tight bite angle of the pyridine-2-carboxamido unit as observed in similar metal complexes with this fragment.[57,78−80] This property is exhibited in Ni-SOD, which also contains acute angles arising from the two five-member chelate rings formed from His1

---

(76) Mills, D. K.; Reibenspies, J. H.; Darensbourg, M. Y. *Inorg. Chem.* **1990**, *29*, 4364.

(77) Krüger, H.-J.; Holm, R. H. *Inorg. Chem.* **1987**, *26*, 3645.

(78) Rowland, J. M.; Olmstead, M. M.; Mascharak, P. K. *Inorg. Chem.* **2002**, *41*, 2754.

(79) Rowland, J. M.; Olmstead, M. M.; Mascharak, P. K. *Inorg. Chem.* **2002**, *41*, 1545.

(80) Rowland, J. M.; Thornton, M. L.; Olmstead, M. M.; Mascharak, P. K. *Inorg. Chem.* **2001**, *40*, 1069.

and Cys2 (Table 1).[15] The relevant bond angles that contain S_{exo} display the most significant changes among the reported complexes, presumably because of the relative degrees of freedom of the non-tethered monodentate thiolate ligand (Table 1). The Ni−S_{exo} bond lengths (avg: 2.193 Å) are more variable differing by 0.042 Å between **2**, which is the longest (2.2139(4) Å) and **5**, which is the shortest (2.172(3) Å). Interestingly, the observed Ni−S_{exo} bond lengths do not appear to be strictly contingent on donor strength of the corresponding thiolate. For example, the Ni−S_{exo} bond of **5** is slightly shorter than **3** (2.1938(7) Å); that of **4** (2.1939(14) Å) is slightly shorter than **2** (2.2139(4) Å) but nearly identical to **3**. It appears that the S_{exo} bond strength in combination with secondary coordination sphere effects (vide infra) play a crucial role in controlling this particular Ni−S bond distance.

Complex **4** (Figure 1), which contains secondary-sphere carboxamide units as part of the S_{exo} donor demonstrate H-bonding in the solid-state based on the N−H group orientation and proximity to sulfur. An intramolecular H-bond is observed in the solid-state structure of **4** and appears to be bifurcated between both thiolate donors with an $N\cdots S_{exo}$ distance of 2.954 Å ($NH\cdots S_{exo}$ = 2.524 Å) and $N\cdots S_{nmp}$ distance of 3.308 Å ($NH\cdots S_{nmp}$ = 2.855) (Figure 1), well below the 3.55 Å sum of the van der Waal's radii of N and S.[81,82] In comparison, the Ni-SOD active site reveals potential H-bonding interactions between Cys6-S and the carboxamide-NH from Val8 and Gly7 ($N\cdots S$ of 3.35 and 3.45 Å, respectively).[15] These N−S distances are comparable to other Ni−SR[74] and Zn−SR[83,84] complexes and synthetic Fe−S clusters[72] with similarly positioned carboxamido-NH functionalities. Interestingly, the solid-state structure of **5** does not reveal any evidence of intramolecular H-bonding as the carboxamide-N(H) is 4.560 Å away from the nearest intramolecular thiolate and clearly directed elsewhere (Figure 2). This observation suggests that the conformation held by an intramolecular H-bond in **5** may be less energetically viable than that which prevails when intermolecular packing forces dominate. Regardless of the presence of H-bonding, both **4** and **5** contain shorter Ni−S_{exo} bond distances than their simple analogues **2** and **3**, respectively. Similar Ni−S bond contractions have been observed in a DFT study of the Ni-SOD active site upon protonation of the thiolates presumably because of the removal of a filled−filled Ni d(π) − S p(π) repulsive interaction.[30]

Previously characterized $Ni^{II}N_2S_2$ complexes such as Ni(bme-daco)[76] and $(Et_4N)_2$[Ni(ema)][23] featuring bis-amine-N and bis-carboxamido-N donors, respectively, employing tetradentate N_2S_2 ligand frameworks serve as suitable benchmarks to compare to **2**−**5**. Additionally, the active site structure of Ni-SOD_{red}[15] (1.3 Å resolution) and the mixed amine/carboxamido $Ni^{II}N_2S_2$ complex (Me_4N)[Ni(BEAAM)] serve as the obvious NiN_2S_2 coordination unit comparison.[37] The Ni−$N_{carboxamide}$ bonds of **2**−**5** appear to be slightly longer than those corresponding to $[Ni(ema)]^{2-}$ and $[Ni(BEAAM)]^{-}$, which are nearly identical at 1.858(6) Å and 1.857(3) Å, respectively, perhaps because of the chelating nature of ema^{4-} and $BEAAM^{3-}$. Unexpectedly, the Ni−$N_{carboxamide}$ bond of Ni-SOD_{red} (2.19(2) Å) appears to be ~0.05 Å longer than those determined for **2**−**5** possibly due to other structural features of the protein secondary and tertiary structure (Table 1). The Ni−N_{amine} bond lengths of Ni(bme-daco) and $[Ni(BEAAM)]^{-}$ are 1.985(6) Å and 1.989(7) Å, respectively, both longer than the Ni−N_{py} lengths for **2**−**5**, suggesting that the pyridyl-N may be a stronger donor than alkylamino-N. The Ni−N_{amine} bond length determined for Ni-SOD_{red} (1.87(6) Å) is strikingly short and more in line with Ni−$N_{carboxamide}$ bonds reported in the aforementioned synthetic complexes.

The Ni−S_{nmp} bonds of **2**−**5** are slightly longer than the Ni−S distance of Ni(bme-daco) and the Ni−S bond trans to the amine of $[Ni(BEAAM)]^{-}$, which are both 2.137(2) Å. The Ni−S_{cys2} bond (trans to the amine) of Ni-SOD_{red} is 2.16(2) Å and the analogous Ni−S distances of **2**−**5** are comparable with this value (Table 1). The Ni−S distances of $[Ni(ema)]^{2-}$ and that trans to the carboxamido-N in $[Ni(BEAAM)]^{-}$ are slightly elongated because of the trans-influence exerted by the strong carboxamido-N σ-donor, 2.179(1) Å and 2.177(2) Å, respectively. Slightly longer Ni−S_{exo} bonds are observed for **2**−**5**, which match well with the Ni−S_{cys6} bond length of 2.19(2) Å in Ni-SOD_{red} (Table 1). It should be noted that the Ni−S_{exo}−C_{α} bond angles of **2**−**5** all deviate significantly from 90°, the optimal angle for thiolate σ-donation to metal centers,[85] despite the unconstrained nature of the monodentate S_{exo} ligands that range from 103.32(6)° for **2** to 119.54(8)° for **3**. Regardless, the Ni−S_{exo} bond lengths for **3** and **5** are quite similar to the analogous Ni−S bonds for $[Ni(ema)]^{2-}$ and $[Ni(BEAAM)]^{-}$, but they possess more acute Ni−S−C_{α} bond angles of 98.1(2)° and 100.3(3)°, respectively. Taken together, complexes **2**−**5** serve as reasonable structural analogues of the asymmetric NiN_2S_2 catalytic unit of Ni-SOD_{red}.

Properties. Complexes **2**−**6** are highly soluble in polar aprotic solvents like MeCN and DMF with partial solubility in non-polar solvents like CH_2Cl_2 and THF (except **6**). Complex **6** is H_2O-soluble but the other complexes remain poorly soluble in H_2O, and all are notably unstable in protic media like MeOH and slowly form dimer **1** upon dissolution. In solvents like MeCN, **2**−**6** form richly colored solutions of varying shades of red-orange arising presumably from Ni-ligand charge-transfer transitions characteristic of square planar $Ni^{II}N_2S_2$ complexes featuring carboxamido-N donors (Figure 3, Table 2).[23,37,86] The λ_{max} values appear to subtly reflect the donor strength of the S_{exo} ligands with transitions occurring at a lower energy for complexes with more strongly donating thiolates. For example, the λ_{max} of **3** is at 464 nm while that of **6** occurs at 442 nm in MeCN at 298 K. Collectively, all of the reported complexes exhibit λ_{max} values centered near the 450 nm value observed for Ni-SOD_{red}.[30] The extinction coefficients

---

(81) Adman, E.; Watenpaugh, K. D.; Jensen, L. H. *Proc. Natl. Acad. Sci. U.S.A.* **1975**, *72*, 4854.

(82) Kato, M.; Okamura, T.; Yamamoto, H.; Ueyama, N. *Inorg. Chem.* **2005**, *44*, 1966.

(83) Chiou, S.-J.; Riordan, C. G.; Rheingold, A. L. *Proc. Natl. Acad. Sci. U.S.A.* **2003**, *100*, 3695.

(84) Morlok, M. M.; Janak, K. E.; Zhu, G.; Quarless, D. A.; Parkin, G. *J. Am. Chem. Soc.* **2005**, *127*, 14039.

(85) Solomon, E. I.; Szilagyi, R. K.; DeBeer George, S.; Basumallick, L. *Chem. Rev.* **2004**, *104*, 419.

(86) Harrop, T. C.; Mascharak, P. K. *Coord. Chem. Rev.* **2005**, *249*, 3007.

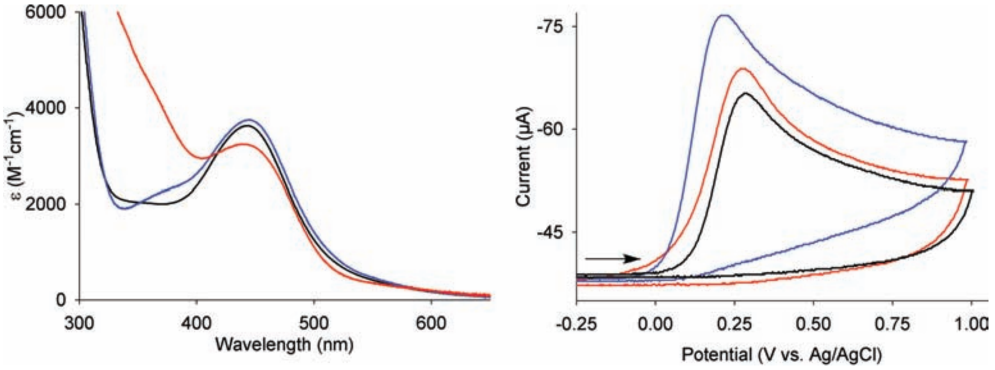

Figure 3. UV–vis spectra of **4** (red), **5** (blue), and **6** (black) in MeCN at 298 K (left). Cyclic voltammograms of 5 mM solutions of **4** (red), **5** (blue), and **6** (black) (vs Ag/AgCl in MeCN, 0.1 M ^{n}Bu$_4$NPF$_6$ supporting electrolyte, glassy carbon working electrode, scan rate: 100 mV/s, RT) (right).

Table 2. Electronic Absorption Spectral Properties and Oxidation Potentials of Complexes **2**–**6** Reported in MeCN at 298 K[a]

	2	**3**	**4**	**5**	**6**
λ_{max} (nm)	450	464	450	449	442
ε (M^{-1} cm^{-1})	5,450	4,540	3,500	3,900	3,710
E_{ox} (mV)	236	75	276	214	286

[a] CVs run in triplicate and represent average values; potentials reported vs Ag/AgCl.

vary from ~3,600– 5,500 M^{-1} cm^{-1} in MeCN, which is consistent with their charge-transfer nature.

Cyclic voltammetry measurements of **2**–**6** reveal irreversible oxidation events in MeCN solvent (vs Ag/AgCl, RT) (Figure 3, Table 2). The irreversibility of the oxidation event is consistent either with primarily ligand-based oxidation or an unstable Ni^{III} species that is short-lived due to autoredox processes. The Ni^{III} state in thiolate-bound coordination complexes is notoriously unstable because of a high propensity for such autoredox processes in which oxidation of the coordinated thiolate to thiyl radical by Ni^{III} eventually affords disulfide and Ni^{II} species.[87] To our knowledge, there are two crystallographically characterized monomeric complexes featuring Ni^{III}-thiolate bonding which can be found in the literature.[88,89] The thiolate ligands in both complexes are within multidentate and bulky ligand frameworks. Thus, the stability of these complexes may be partially attributed to the chelate effect and steric factors, which complexes **2**–**6** presently lack. The oxidation potentials of **2**–**6** all fall in between values obtained for structurally similar bis-amino dithiolate[28] and bis-carboxamido dithiolate[23] Ni^{II}N$_2$S$_2$ complexes. In general, a comparison of the oxidation potentials (E_{ox}) of **2**–**6** appears to reflect the donor strength of S$_{exo}$ when aryl- and alkyl-thiolate donors are analyzed separately. For example (looking at the aryl-S complexes **2** and **4**), complex **2** containing the mildly electron withdrawing *p*-chloro functionality oxidizes at 236 mV, 40 mV less than **4** (E_{ox} = 276 mV in MeCN). This cathodic shift may be attributed to the sequestration of the electron donating ability of the S-*o*-babt ligand by intramolecular NH···S bonding similar to other carboxamido modified thiolates. Indeed, Hammett constants indicate the Cl group (σ_p = 0.227) to be more electron withdrawing than the benzamide group (σ_p = 0.078).[90] The difference of 40 mV in E_{ox} of **2** and **4** is somewhat low in light of results obtained by Ueyama regarding aryl substituent effects on the oxidation potentials of [Fe$_2$S$_2$(SR)$_4$]$^{2-}$ clusters featuring variable thiolate ligands.[72] For example, comparing the $E_{1/2}$ of [Fe$_2$S$_2$(SPh)$_4$]$^{2-}$ with [Fe$_2$S$_2$(S-*o*-CH$_3$NHCOC$_6$H$_4$)$_4$]$^{2-}$ (σ_p = −0.015) effected a 140 mV cathodic shift of $E_{1/2}$ in MeCN.[72] Perhaps this greater shift in the Fe–S clusters is an additive value reflected in the total number of H-bonds in the cluster (4 H-bonds), which on a per H-bond analysis (35 mV cathodic shift/H-bond) would be similar to what is observed in our systems. A similar trend is observed in the oxidation potentials of complexes **3**, **5**, and **6** featuring alkyl S$_{exo}$ donors as the anodic events of **5** and **6** appeared at 214 mV and 286 mV while that of **3** arises at 75 mV. The influence of H-bonding is quite evident in the alkyl-thiolate (e.g., more cysteine-like) donors resulting in a ~200 mV cathodic shift upon incorporation of the H-bonding moieties in **5** and **6** with respect to the non H-bonded complex **3**. Thus, a stronger induced dipole from the H-bond in the alkyl systems results in a significant cathodic shift. These H-bonded analogues are close to the protein midpoint potential value of 490 mV (vs Ag/AgCl, pH 7.5 phosphate buffer)[24] and indicate that these complexes are electrochemically feasible for performing SOD chemistry but do not yet demonstrate electrochemical reversibility.

The ^{1}H NMR spectral data of complexes **2**–**6** are consistent with retention of square planar coordination as all exhibit diamagnetic (S = 0, d^8) spectra in both non-donor and donor aprotic solvents. The H-bonding interactions of **4**, **5**, and **6** are all evident from ^{1}H NMR spectroscopy and are reflected in the change of the NH chemical shift (δ_{NH}) in the free versus complexed ligand. In all the complexes, δ_{NH} is significantly shifted downfield relative to δ_{NH} arising from the monodentate S$_{exo}$-ligand when unbound to the Ni(nmp) unit.[83,84] For example, δ_{NH} of S-*o*-babt-disulfide, HS-meb, and HS-NAc occur at 8.95 ppm in CDCl$_3$, 6.74 ppm in CDCl$_3$ and 7.43 ppm in d_6-acetone, respectively. The corresponding NH peaks in **4**, **5**, and **6** appear at 10.57 ppm in CDCl$_3$, 8.52 ppm in CDCl$_3$, and 8.73 ppm in d_6-acetone, respectively (Figure 4, Table 3). Thus, the presence of intramolecular H-bonding places NH protons in a more deshielded electronic environment as a result of a weakened interaction with the electronegative carboxamido-N. The large shift observed for **5** (nearly 2 ppm)

---

(87) Stenson, P. A.; Board, A.; Marin-Becerra, A.; Blake, A. J.; Davies, E. S.; Wilson, C.; McMaster, J.; Schröder, M. *Chem.—Eur. J.* **2008**, *14*, 2564.

(88) Fox, S.; Wang, Y.; Silver, A.; Millar, M. *J. Am. Chem. Soc.* **1990**, *112*, 3218.

(89) Hanss, J.; Krüger, H.-J. *Angew. Chem., Int. Ed.* **1998**, *37*, 360.

(90) Jaffé, H. H. *Chem. Rev.* **1953**, *53*, 191.

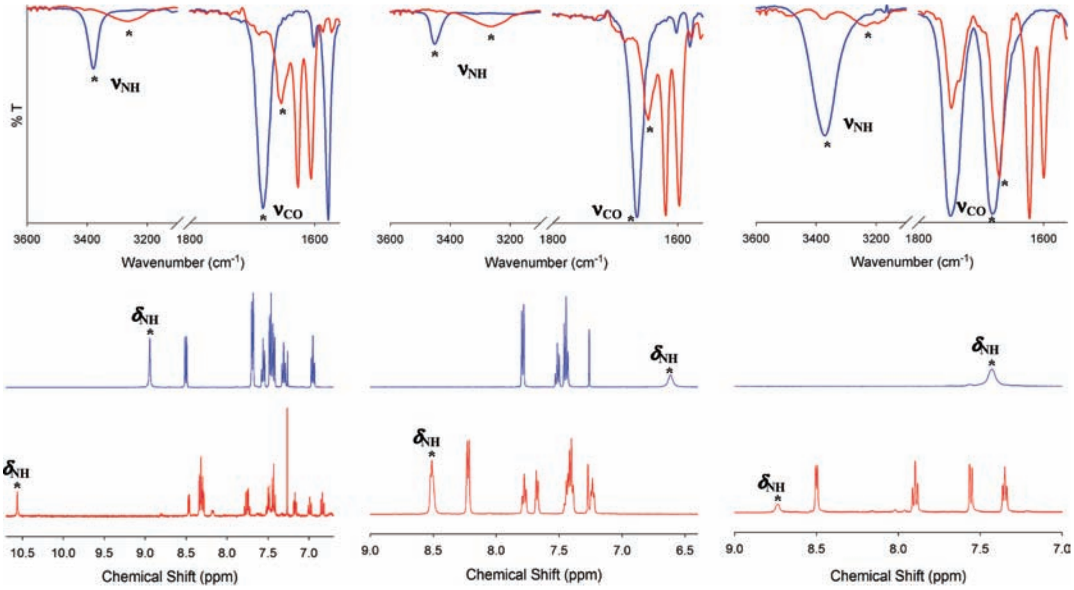

Figure 4. Comparison of shifts in the ν_{NH}, ν_{CO} of the carboxamide, and δ_{NH} (denoted by *) of the disulfide or thiol forms of S_{exo} ligands (blue) and upon complexation to the Ni(nmp) unit (red) by solution FTIR (top) and ^{1}H NMR (bottom). Left: **4** and disulfide of S-*o*-babt (IR in CH_2Cl_2, ^{1}H NMR in $CDCl_3$). Center: **5** and HS-meb (IR in CH_2Cl_2, ^{1}H NMR in $CDCl_3$). Right: **6** and HS-NAc (IR in MeCN, ^{1}H NMR in CD_3CN).

is indicative of a particularly strong intramolecular H-bond for this complex in solution.[82]

Table 3. Changes in the ^{1}H NMR Chemical Shift (ppm) of δ_{NH} and IR Stretching Frequencies (cm^{-1}) of ν_{CO} and ν_{NH} of the Carboxamide Group of S_{exo} Ligands upon Binding to the Ni(nmp) Metallosynthon (^{a}CDCl$_3$, ^{b}CH$_2$Cl$_2$, ^{c}CD$_3$CN, ^{d}MeCN Recorded at 298 K)

	o-babt-S_2	**4**	HS-meb	**5**	HS-NAc	**6**
δ_{NH}	8.95^a	10.57^a	6.74^a	8.52^a	7.43^c	8.73^c
$\Delta\delta_{NH}$		1.63		1.78		1.30
$\nu_{NH\ (liquid)}$	3379^b	3274^b	3452^b	3261^b	3371^d	3235^d
$\Delta\nu_{NH\ (liquid)}$		−105		−191		−136
$\nu_{CO\ (liquid)}$	1682^b	1670^b	1665^b	1647^b	1682^d	1671^d
$\Delta\nu_{CO\ (liquid)}$		−12		−18		−11
$\nu_{NH\ (KBr)}$	3374, 3326	3271	3299	3298	3307	3264
$\Delta\nu_{NH\ (KBr)}$		−103, −55		−1		−43
$\nu_{CO\ (KBr)}$	1680	1652	1634	1643	1644	1662
$\Delta\nu_{CO\ (KBr)}$		−28		9		18

The FTIR spectra of the complexes are indicative of the coordination of deprotonated carboxamido-N from the noted red-shift of the ν_{CO} band from 1658 cm^{-1} in the free nmpH$_2$ ligand to 1574−1623 cm^{-1} in **2**−**6**. The FTIR spectra of complexes **4**−**6** in solid- and/or solution-state provide clear evidence for the formation of intramolecular H-bonds from the S_{exo} thiolate ligands by monitoring changes in the ν_{NH} and ν_{CO} stretching frequencies of the complexed S_{exo} ligands (Table 3, Figure 4). Evidence for H-bond formation is further supported through the NMR data (see above). Solution IR measurements corroborate the downfield shifts of the NH proton resonance observed in the ^{1}H NMR of **4**−**6** and confirm the presence of H-bonding interactions in solution. For example, the ν_{NH} of S-*o*-babt disulfide appears at 3379 cm^{-1} whereas the ν_{NH} arising from **4** appears as a broad red-shifted peak at 3274 cm^{-1} (Figure 4, left). The solid-state FTIR spectrum (KBr pellet) reveals similar trends demonstrative that NH···S bonding interactions are present in the solid-state as well (Table 3). This ~100 cm^{-1} red-shift in ν_{NH} is also observed in H-bonded synthetic Fe−S clusters[72] and square planar Pt^{II}N$_2$S$_2$[82] complexes bearing *ortho*-benzamido thiolate donors. The difference between the solution NH stretching frequency for HS-meb and **5** is particularly striking. The ν_{NH} appears as a sharp peak at 3452 cm^{-1} for the free thiol and is red-shifted by ~200 cm^{-1} (3261 cm^{-1}) in complex **5** (Figure 4, center). The dramatic difference in ν_{NH} is again indicative of the formation of a relatively strong intramolecular H-bond[72] in **5** that is consistent with the observed downfield shift of the NH proton in the ^{1}H NMR spectrum (Figure 4, center). The analogous stretches in MeCN appear at 3396 cm^{-1} for HS-meb and 3273 cm^{-1} for **5** implying that H-bonding interactions in **5** may be slightly less ($\Delta\nu_{NH}$: 123 cm^{-1}) in polar solvents but of similar magnitude. Consistent with the crystal structure of **5**, the FTIR revealed no evidence for intramolecular H-bonding in the solid-state as ν_{NH} of HS-meb and **5** appeared at nearly identical values, 3299 cm^{-1} and 3298 cm^{-1}, respectively. The signature frequencies and shifts associated with intramolecular H-bonding are observed in both the solid- and the solution-state FTIR spectra of **6** (Table 3, Figure 4, right). The H-bonding interactions in **4**−**6** are also evident, albeit to a lesser extent, in the stretching frequencies of the carbonyl (ν_{CO}) region of the exogenously appended amido-thiolate ligand (Table 3, Figure 4). For example, the ν_{CO} of S-*o*-babt disulfide and HS-meb shift from 1682 cm^{-1} and 1665 cm^{-1} to 1670 cm^{-1} and 1647 cm^{-1} in CH$_2$Cl$_2$ upon complexation in **4** and **5**, respectively ($\Delta\nu_{CO}$ = 12−18 cm^{-1}). Similar changes are also observed in polar solvents like MeCN.

O_2(g), H_2O_2, and $O_2^{\bullet -}$ Reactivity. The interaction of our model systems with ROS and O$_2$ is crucial for understanding how Ni-SOD avoids formation of unwanted sulfur−oxygenates or disulfide during catalysis. Proposals of cysteine protonation and/or H-bonding interactions in Ni-SOD have been implicated to protect the coordinated thiolates from such oxidative modification.[30,38] For example, electronic structure calculations by Brunold on truncated models of the Ni-SOD active site displayed a 0.03 Å contraction of the Ni−S bond upon S-protonation attributed to decreased antibonding S-character in the HOMO.[30] An additional DFT study by Grapperhaus on

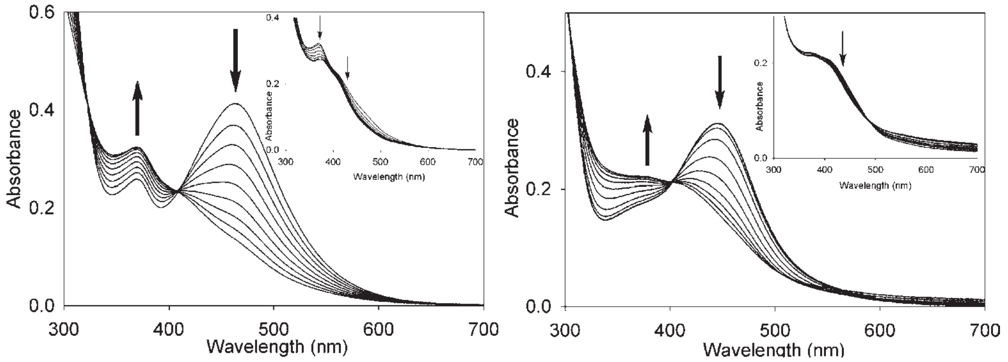

Figure 5. Disappearance of λ_{max} = 464 nm of **3** and λ_{max} = 449 nm of **5** in MeCN (0.13 mM) with concurrent rise and appearance of peaks at 370 and 373 nm, respectively, after 2 h exposure to O_2(g) at 298 K. Inset: decay of resultant spectra over the next 2 h under identical conditions.

computer generated Ni-SOD models suggested that H-bonding to thiolates imparts a stabilizing effect due to a more positive electrostatic potential around the coordinated thiolates. Thus, H-bonding localizes most of the charge at the Ni center supporting a decrease in nucleophilic character on the H-bonded sulfur and a low propensity for S to react with oxidants.[25] This H-bond, however, does not appear to change the overall nature of the HOMO composition although the contribution from the H-bonded S-donor drops significantly (15% to 5%). In this regard, we were interested to experimentally validate these H-bond effects, if any, by treating complexes **2**−**6** with excess O_2, H_2O_2, and $O_2^{\bullet-}$.

The reaction of the Ni complexes **2**−**6** with excess O_2(g) was performed at 298 K and initially monitored by UV−vis spectroscopy. The characteristic charge-transfer band of the Ni^{II} complexes was the principle feature to monitor and served as the indicator of complex consumption/S-modification.[27,46] UV−vis spectra were acquired every 15 min after addition of O_2(g) for a total time of 4 h in MeCN. The characteristic intense ~450 nm band of these complexes diminished rather slowly resulting in notable isosbestic behavior in some systems and new blue-shifted peaks in the 370−400 nm range (see Figure 5 for complexes **3** and **5** and Figures S4−S8 in the Supporting Information for others). For example, the UV−vis reaction profile of **3** revealed a clean transition within the first 2 h of O_2 addition to what we tentatively assign as a Ni−SO_2 species (see below) with an isosbestic point at 405 nm and a blue-shifted broad feature at 370 nm (Figure 5). The last 2 h of the reaction did not display isosbestic behavior and resulted in decreased intensity of these peaks that are consistent with complex degradation. Similar behavior was observed for the other Ni complexes (see the Supporting Information).

The relatively sluggish reaction profile under pseudo first-order conditions for these systems is consistent with reports of other square planar Ni^{II} complexes in similar coordination environments (vide infra). The observed rate constants (k_{obs}) were on the order of 10^{-4} s^{-1} for complexes **3**−**6** (Table 4 and the Supporting Information), while **2** decays a full order of magnitude slower, k_{obs} = 4.22 ± 0.69 × 10^{-5} s^{-1}. Although we have not performed detailed mechanistic studies on these reactions, the FTIR spectra of the concentrated reaction mixtures after 4 h of O_2 exposure revealed formation of S-oxygenates (Supporting Information, Figure S14). For example, the alkyl systems **3**, **5**, and **6** displayed intense ν_{SO} bands in the IR near ~1100 and 1050 cm^{-1} consistent with S-oxygenate formation. Unfortunately, attempts at determining the exact nature of the end products (by ESI-MS, ^{1}H NMR, solvent extraction of products) have thus far been unsuccessful. It does appear, however, that under the forcing conditions employed, the O_2 reaction resulted in products beyond simple S-oxygenation (Figure 5 inset shows decay). The UV−vis in combination with ESI-MS data initially indicated a clean transformation to one new species that we hypothesize to be a Ni−SO_2 species based on literature precedent.[27,46,91] Upon completion of the UV−vis experiment for **5**, small amounts of precipitate appeared, which have been confirmed as the dimeric species **1**. DFT (vide infra) calculations suggest that the S_{exo} would be the most likely candidate for oxygenation being the more nucleophilic of the two S-donors, and formation of the S,S-bridged complex **1** would be precluded if oxygenation had occurred at S_{nmp}. More direct evidence supporting S_{exo}-oxygenation have come from high-resolution ESI-MS data where species with mass assignments corresponding to the free sulfinate (RSO_2^-) and sulfonate (RSO_3^-) of the S-meb$^-$ ligand were observed under identical conditions as the O_2 UV−vis experiments with **5** (see the Supporting Information, Figure S15).

Table 4. Pseudo First-Order Kinetic Rate Constants (k_{obs} in s^{-1}) of Complexes **2**−**6** upon Exposure to Excess O_2(g) (~60 mol-equiv) over 4 h and H_2O_2 (20 mol-equiv) over 5 min in MeCN at 298 K

complex	O_2	H_2O_2
2	4.22 ± 0.69 × 10^{-5}	1.27 ± 0.07 × 10^{-2}
3	2.61 ± 0.65 × 10^{-4}	5.77 ± 0.66 × 10^{-2}
4	1.63 ± 0.03 × 10^{-4}	1.32 ± 0.39 × 10^{-2}
5	2.13 ± 0.04 × 10^{-4}	1.04 ± 0.04 × 10^{-2}
6	1.77 ± 0.09 × 10^{-4}	1.59 ± 0.09 × 10^{-2}

The reactions with H_2O_2 were performed in a similar fashion to that described for the O_2(g) reactions. As expected, these reactions are less discriminate and significantly faster than with O_2(g). Addition of 20 equiv of H_2O_2−urea (pseudo first-order conditions) to MeCN solutions of **2**−**6** at 298 K resulted in a rapid bleaching of the solution and a decrease in the charge-transfer band coupled with a shift of λ_{max} to higher energy in each subsequent scan, presumably reflective of S-oxygenate formation as initial UV−vis traces are comparable to the O_2(g) reactions (in the Supporting Information, Figures S9−S13). Complexes **2**−**6** show little variation in the reaction rate,

---

(91) Hatlevik, Ø.; Blanksma, M. C.; Mathrubootham, V.; Arif, A. M.; Hegg, E. L. *J. Biol. Inorg. Chem.* **2004**, *9*, 238.

and all k_{obs} are on the order of 10^{-2} s^{-1} with complexes **3** and **5** displaying the most rapid and slow kinetics, respectively (Table 4). Complex **3** decays at $k_{obs} = 5.77 \pm 0.66 \times 10^{-2}$ s^{-1} and **5** at $k_{obs} = 1.04 \pm 0.04 \times 10^{-2}$ s^{-1}. Thus, H-bonding does provide a modest (~6-fold) degree of protection in the alkyl systems. Similar rate modification has been noted with Zn^{II}-coordinated H-bonded thiolates upon reaction with CH_3^+.[92] The FTIR spectra of concentrated reaction mixtures of H_2O_2(aq) treated **2**−**6** revealed strong ν_{SO} bands similar to those seen after prolonged O_2(g) exposure (Supporting Information, Figure S14) except with more intense peaks in the 1300−1400 cm^{-1} region consistent with RSO_3^- formation (i.e., complete ligand S-oxygenation).

Complexes **2**−**6** were also examined for $O_2^{\bullet -}$ reactivity under similar conditions as performed for O_2(g) and H_2O_2. Addition of up to 12 equiv of KO_2 (solubilized in THF with 18-crown-6) at 298 K to MeCN solutions of the Ni complexes **2**, **3**, **5**, and **6** resulted in negligible changes in their corresponding UV−vis spectra. Perhaps the inability to stabilize Ni^{III} and the lack of a fifth axial-N-donor, shown to be critical for enzyme activity,[15,30,32] may contribute to the non-reactivity of these systems. Furthermore, addition of excess (10 mol-equiv) imidazole to MeCN solutions of **2**−**6** result in no major changes to the UV−vis spectra suggesting no enhanced $O_2^{\bullet -}$ reactivity even in the presence of a potential N-donor. The immediate proximity of His1 to the Ni center of Ni-SOD presumably leads to immediate binding during catalysis,[15] whereas our systems do not benefit from any enhanced proximity to force coordination. Regardless, it is evident that $O_2^{\bullet -}$ lacks an affinity for **2**, **3**, **5**, and **6** under these conditions. However, a distinct spectral change is observed in the UV−vis spectrum of **4** with the addition of 45 equiv of KO_2 (see Supporting Information, Figure S16). It should be noted that the changes observed are instantaneous and do not seem to change over the course of 1 h, indicative that the new species formed is stable in solution at 298 K. Additionally, 10 equiv of imidazole does not provide any notable effect on this reaction. ESI-MS did not reveal any Ni-superoxo species as only starting material was observed. Unfortunately, the general instability of the Ni complexes in protic media presents a limitation toward probing their chemistry in the presence of $O_2^{\bullet -}$ in aqueous conditions excluding the traditional NBT/formazan assay.[45] Instead we probed the reactivity of **4** with the azide ion (N_3^-) as a superoxide analogue. Similar changes to the spectrum of **4** are observed upon treatment with 12 equiv of N_3^- under identical conditions. Analysis of the N_3^- reaction with **4** by ESI-MS revealed the presence of $[Ni(nmp)(N_3)]^-$ as well as the anionic portion of unreacted **4**, but no peaks corresponding to a five-coordinate azido-species like $[Ni(nmp)(S\text{-}o\text{-}babt)(N_3)]^{2-}$ were found (see Supporting Information, Figure S16). It should be noted that the addition of 12 equiv of N_3^- to **2**, **3**, **5**, and **6** under identical conditions resulted in no UV−vis spectral changes. It is presumed that excess $O_2^{\bullet -}$ interacts with **4** via ligand substitution for S_{exo} presumably because of the relative weakness of this Ni−S_{exo} bond especially under these forcing conditions. The redox innocence of $O_2^{\bullet -}$ seems likely in the aprotic environment, and the resulting spectra of N_3^- treated **4** afforded similar features; however, the exact nature of the interaction remains unresolved at present.

The Ni^{II} complexes **2**−**6** all react when treated with the SOD products H_2O_2 or O_2(g) under forcing conditions at 298 K with a small variation in k_{obs} when reactivity with the two oxidants are analyzed separately. Such reactivity is important to understand considering the unusual nature of the Ni-SOD active site. Furthermore, there are few reports regarding the reaction kinetics of Ni-bound thiolates toward H_2O_2 or O_2(g) to compare our results[93] and none regarding Ni-SOD synthetic analogues. Numerous literature precedents suggest that the oxidative degradation of **2**−**6** most likely involves O-modification of the thiolate ligands to form SO_x species (where x = 1, 2, or 3 for sulfenato, sulfinato, and sulfonato groups, respectively).[27,28,46,91] Examination of the reaction products by ESI-MS, FTIR, and UV−vis spectroscopies have provided some evidence for the formation of such species although an exact product distribution has yet to be established. The O_2(g) reactivity rates for **2**−**6** are similar to those observed for structurally analogous Ni^{II} complexes bearing in mind the disparity in recording temperature. For example, the k_{obs} for excess O_2(g) reactions with anionic $[Ni^{II}(NS_2)(CN)]^-$ and neutral $Ni^{II}NS_3$ complexes are reported to be 10^{-4} s^{-1} and 10^{-6} s^{-1}, respectively in DMF at 313 K.[93,94] The rate differences have been attributed in part to the difference in nucleophilicity of the terminal thiolates between the anionic and the neutral complexes and suggest Ni-SOD_{red} and Ni-SOD_{ox} should also exhibit different, albeit very slow, rate profiles with O_2. Analogous rates have also been observed for the reaction of excess CH_3^+ with Zn^{II}-bound thiolates in MeCN at 298 K.[92,95] In these studies, intramolecular NH···S H-bonding slows k_{obs} by a full order of magnitude in some cases.[92,95] Extrapolating mechanistic data from the corresponding kinetic information of S-oxygenation, however, is more complicated than that of methylation.[93,96,97] Additionally, the presence of a second coordinated thiolate in **2**−**6** provides an even less controlled situation,[27] rendering a detailed mechanistic analysis beyond the scope of the present work. Also, the possibility of a mechanistic pathway other than nucleophilic attack of O_2 or H_2O_2 by a thiolato-S has not been ruled out for the systems presented here. The degree to which the active site of Ni-SOD is exposed to H_2O_2, O_2, and $O_2^{\bullet -}$ is largely unknown and some debate continues over an inner- versus outer-sphere mechanism for Ni-SOD[30,32,42] with the latter being the more appealing and most probable choice. A recent site directed mutagenesis study on Ni-SOD demonstrated the importance of Tyr9 as a "gatekeeper" residue resulting in H_2O_2 saturation kinetics upon mutation. This residue is proposed to direct substrate access and minimize H_2O_2 build-up around the active site via an efficient

---

[92] Smith, J. N.; Hoffman, J. T.; Shirin, Z.; Carrano, C. J. *Inorg. Chem.* **2005**, *44*, 2012.

[93] Mirza, S. A.; Pressler, M. A.; Kumar, M.; Day, R. O.; Maroney, M. J. *Inorg. Chem.* **1993**, *32*, 977.

[94] Mirza, S. A.; Day, R. O.; Maroney, M. J. *Inorg. Chem.* **1996**, *35*, 1992.

[95] Smith, J. N.; Shirin, Z.; Carrano, C. J. *J. Am. Chem. Soc.* **2003**, *125*, 868.

[96] Tuntulani, T.; Musie, G.; Reibenspies, J. H.; Darensbourg, M. Y. *Inorg. Chem.* **1995**, *34*, 6279.

[97] Buonomo, R. M.; Font, I.; Maguire, M. J.; Reibenspies, J. H.; Tuntulani, T.; Darensbourg, M. Y. *J. Am. Chem. Soc.* **1995**, *117*, 963.

removal mechanism.[24] The rapid H_2O_2 kinetics and resulting decomposition of our models, which lack the protective environment of the protein supports the need for such a mechanism. Collectively, this data is consistent with the notion that the Ni-SOD active site is kinetically protected from adventitious reaction with $O_2(g)$.[31] Although little mechanistic insight can be deduced from the O_2 and H_2O_2 experiments, it is clear that our "stripped" $Ni^{II}N_2S_2$ active site analogues are relatively stable to excess $O_2(g)$ but unstable toward excess H_2O_2 at 298 K.

Electronic Structure. DFT computations were employed to obtain electronic descriptions of the Ni-SOD model complexes. Previous DFT accounts on Ni-SOD models have focused on the role of the mixed amine/carboxamido-N coordination sphere, where it was concluded that the presence of the mixed N-ligands supports Ni-based redox chemistry to protect the active site from S-based oxidation.[30,34] Other DFT studies have focused on the impact of H-bonded H_2O molecules (absent in Ni-SOD) in $Ni^{II}N_2S_2$ and $Fe^{II}N_4S$ complexes establishing the passive versus active nature of H-bonding in these discrete systems.[98] The present research therefore offers the first opportunity to look at S-based modification (H-bonding) of synthesized small molecule analogues directly related to Ni-SOD from both an experimental and a theoretical approach. The initial coordinates for complexes **2**−**5** were obtained from the X-ray structures (that of **6** from an estimate utilizing coordinates from **3**), and the geometries were optimized with the OLYP functional (def2-TZVPP basis set). A full summary of the optimized structures including NBO atomic charges, electrostatic potentials (ESPs), and relevant atomic coordinates can be found in Table 5 and with complete detail in the Supporting Information. The geometry optimizations of **2**−**6** compare well with the experimentally determined metric parameters (Figure 6 for **3** and **5**, Supporting Information, Figures S17−S21 and Supporting Information, Tables S7−S8 for the rest). The optimized models reproduce the coordination geometry with small overestimates in the Ni−L bond lengths, providing bond distances within 0.05 Å of the experimental values. The overestimate in bond lengths is well within the accuracy of the OLYP functional. It is important to note that DFT replicates the asymmetric nature of the different N-donors in **2**−**6** and is consistent with the strong ligand-field of the carboxamido-N versus the pyridine-N donor. Additionally, the optimized models accurately replicate the longer Ni−S bond length from the monodentate S_{exo}-donor. The only noteworthy divergence is found for **5**, which DFT optimizes to include the presence of an intramolecular NH···S H-bond (Figure 6). The latter result is not too surprising considering this H-bond interaction has been established in solution (vide supra). Collectively, the accuracy with which the structures generated by DFT replicate the experimental metric parameters validates the computations employed in the present work.

Table 5. Relevant Bond Lengths (Å), Bond Angles (deg), Atomic Charges, and Electrostatic Potentials (ESPs) (a.u.) of DFT Geometry Optimized Structures of Complexes **2**−**6**

	2	3	4	5	6
$Ni-N_{am}$	1.891	1.905	1.891	1.895	1.897
$Ni-N_{py}$	1.955	1.961	1.955	1.959	1.960
$Ni-S_{nmp}$	2.156	2.160	2.156	2.166	2.167
$Ni-S_{exo}$	2.239	2.253	2.253	2.224	2.228
$N_{pep}\cdots S_{exo}$			2.935	3.209	3.106
$N_{pep}-H$			1.022	1.012	1.018
$N_{pep}-H\cdots S_{exo}$			2.271	2.729	2.533
$N_{am}-Ni-N_{py}$	82.7	82.3	82.8	82.7	82.6
$N_{am}-Ni-S_{nmp}$	88.7	88.4	88.5	87.9	87.7
$N_{am}-Ni-S_{exo}$	173.9	178.3	175.2	175.2	176.4
$N_{py}-Ni-S_{nmp}$	170.7	170.6	171.2	170.3	170.2
$N_{py}-Ni-S_{exo}$	98.6	97.0	97.9	93.5	94.3
$S_{nmp}-Ni-S_{exo}$	90.3	92.3	90.9	96.1	95.4
$Ni-S_{nmp}-C\alpha$	98.1	97.8	98.0	98.2	97.8
$Ni-S_{exo}-C\alpha$	111.9	113.5	112.1	117.4	113.1
$N_{pep}-H\cdots S_{exo}$			121.3	109.4	115.2
atomic charge N_{am}	−0.56	−0.57	−0.56	−0.56	−0.56
atomic charge N_{py}	−0.43	−0.43	−0.43	−0.42	−0.42
atomic charge S_{nmp}	−0.23	−0.25	−0.24	−0.29	−0.28
atomic charge S_{exo}	−0.18	−0.34	−0.26	−0.38	−0.35
atomic charge Ni	0.62	0.63	0.63	0.64	0.64
ESP S_{nmp} (a.u.)	−59.4286	−59.4404	−59.4237	−59.4260	−59.4277
ESP S_{exo} (a.u.)	−59.4201	−59.4518	−59.4114	−59.4280	−59.4245

Insight into the influence of H-bonding on the metric parameters of **4**−**6** can be gained from the DFT calculated structures. Optimized models of **5** and **6** reveal a contraction of the $Ni-S_{exo}$ bond by ~0.03 Å versus **3** upon formation of intramolecular H-bonds with concurrent shortening of the $Ni-N_{carboxamide}$ bond by ~0.01 Å, which is reflective of charge neutralization of the trans thiolate (Figure 6, Table 5, and Supporting Information, Figure S21). The $Ni-S_{exo}$ bond contraction observed by DFT and in the structure of **4** has been postulated to be due to a decrease in the filled/filled repulsive interaction between the Ni(dπ) and S(pπ) orbitals upon H-bond formation. A study of in silico Ni-SOD_{red} models revealed a similar contraction in an H-bonded S-ligand of the same magnitude.[25] Additionally, a DFT study on a truncated model of the Ni-SOD_{red} active site reveals contraction of the Ni−S bond distance upon protonation of Cys6 or Cys2 by ~0.03 Å.[30] All H-bonding interactions observed in the DFT generated structures are clearly directed toward S_{exo}, as a result of the strong trans influence of the carboxamido-N, in addition to the orientation and proximity of the NH to S_{exo}. The distances between S_{exo} and the N of the appended carboxamide range from 2.935 Å (**4**) to 3.209 Å (**5**) and are slightly less than the N···S distances between Cys6 with Val8 (3.35 Å) and Gly7 (3.45 Å) in Ni-SOD.[15] This result is likely due to the absence of other secondary interactions present in the enzyme. However, a similar $N-S_{exo}$ bond length of 2.954 Å is observed in the X-ray crystal structure of **4** (Figure 1, Table 1),

The important issues to address regarding Ni-SOD function is how the enzyme avoids S-based oxygenation in the presence of O_2 and ROS and how Ni^{III} is stabilized during catalytic turnover without resulting in S-oxidation. A partial solution lies in the electronic structural description of the active site and relevant synthetic analogues. A number of descriptors, such as HOMO composition,[30] atomic charges, and ESPs[25] can be envisaged to determine the preference for oxidation at the Ni center or the ligands. The key bonding features of the frontier MOs, as well as the percent Ni- and S-contribution to these MOs, are displayed in Figure 7, Tables 6−8, and in the

---

(98) Dey, A.; Green, K. N.; Jenkins, R. M.; Jeffrey, S. P.; Darensbourg, M.; Hodgson, K. O.; Hedman, B.; Solomon, E. I. *Inorg. Chem.* **2007**, *46*, 9655.

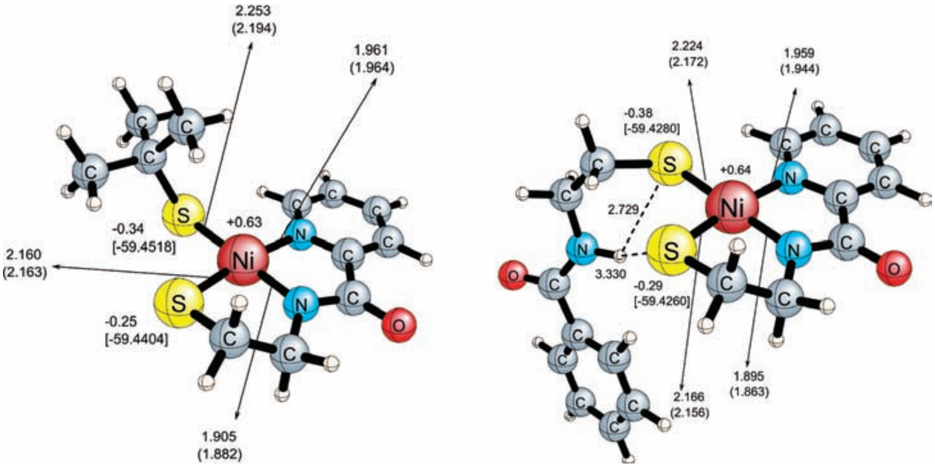

Figure 6. Geometry optimized structures of complexes **3** (left) and **5** (right) featuring relevant bond distances (crystallographically determined distances shown in parentheses), NBO atomic charges, and electrostatic potentials at relevant nuclei [in a.u. shown in brackets].

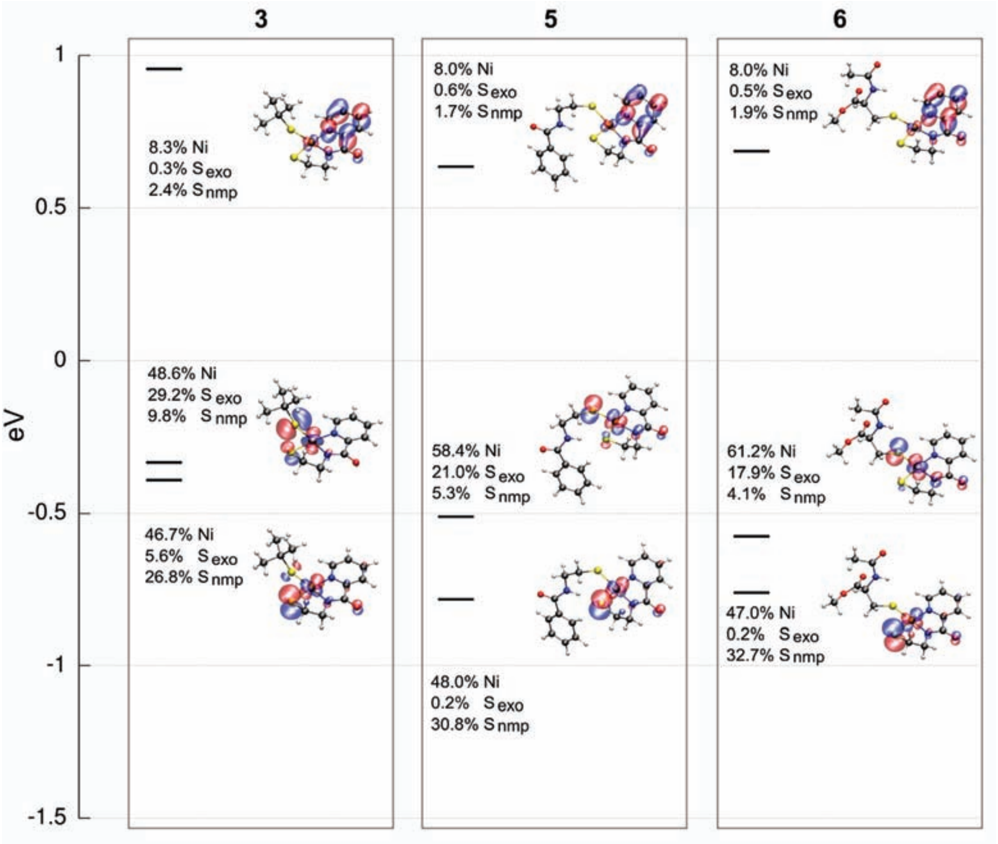

Figure 7. DFT generated isosurface plots of the frontier MOs of the geometry optimized structures of the alkyl S_{exo} complexes **3**, **5**, and **6**. In each column, the orbitals descend in the order LUMO, HOMO, and HOMO-1.

Supporting Information. For all complexes, the lowest unoccupied molecular orbital (LUMO) remains π-antibonding between the C(pπ) orbitals on the pyridine ring of the nmp ligand. The nature of the HOMO and HOMO-1 principally involve π-antibonding interactions between the S-π-orbitals and the Ni d-π-orbitals, reflecting the high degree of covalency in the Ni−S bond of these complexes. If we separately analyze the series containing *alkyl* S_{exo} ligands, ordered by decreasing electron releasing capability, a clear trend emerges among the HOMO compositions. Within this series, the Ni contributions of **3**, **5**, and **6** increase to 48.6%, 58.4%, and 61.2%, respectively, accompanied by a decrease in contributions from S_{exo} (and total S) to 29.2% (39.0% total S), 21.0% (26.3% total S), and 17.9% (22.0% total S), respectively (Figure 7, Tables 6−8). The close lying HOMO-1 for **3** (46.7% Ni; 32.4% total S), **5** (48.0% Ni; 31.0% total S), and **6** (47.0% Ni, 32.9% total S) also contains mostly Ni-character. *This trend implies that decreased electron density at the coordinated alkyl thiolate increases the feasibility of metal-based redox*. Surprisingly, the NBO atomic charges on the exogenous thiolates of **3**, **5**, and **6** correspond to −0.34, −0.38, and −0.35, respectively, and do not reflect this trend. The charges on the Ni center remain essentially constant as well and 0.63, 0.64, and

Table 6. Löwdin Orbital Compositions Derived from the DFT Calculations for Selected Molecular Orbitals of Complex **3**

MO label	MO	*E* (eV)	%Ni[a]	%N[b]	%S[c]	orbital composition
LUMO[d]	86	0.95	8.3	18.8	2.7	$Ni(d_{xz}) - N_{py}(p_z), N_{am}(p_z)$
HOMO	85	−0.34	48.6	1.9	39.0	$Ni(d_{yz})/Ni(d_{xz}) - S_{exo}(p_x), S_{nmp}(p_z)$
HOMO-1	84	−0.40	46.7	2.7	32.4	$Ni(d_{xz})/Ni(d_{yz}) - S_{nmp}(p_z)$
HOMO-2	83	−0.59	88.7	2.7	3.6	$Ni(d_{z2})$
HOMO-3	82	−0.68	54.0	5.4	26.7	$Ni(d_{yz})/Ni(d_{xy}) - N_{am}(p_z), S_{exo}(p_x)$
HOMO-4	81	−1.58	32.8	4.9	38.2	$Ni(d_{xz}), N_{am}(p_y)/N_{am}(p_z), S_{nmp}(p_z)/S_{nmp}(p_y), S_{exo}(p_y)/S_{exo}(p_z)/S_{exo}(p_x)$
HOMO-5	80	−1.73	32.7	3.7	30.6	$Ni(d_{xy}) + N_{am}(p_y)/N_{am}(p_x), S_{exo}(p_x)/S_{exo}(p_z)$
HOMO-6	79	−1.90	30.4	9.2	13.9	$Ni(d_{xy})/Ni(d_{yz}) + N_{am}(p_z)/N_{am}(p_x), S_{nmp}(p_z)/S_{nmp}(p_y)$

[a] MO contribution from the Ni AOs. [b] MO contribution from the N AOs of N_{py} and the coordinated $N_{carboxamide}$. [c] MO contribution from the S AOs. The composition is given in order of AO contribution to the MO. [d] The major contributions to the LUMO involves C(pπ) AOs from the pyridine ring of nmp (56.2%). Bonding interactions are represented with a + and antibonding interactions are denoted with a −. The coordinate system used for figuring out the type of AO on Ni, N, and S are as follows: *z*-axis is normal to the square planar ligand field; *x*-axis is parallel to $S_{nmp}-Ni-N_{py}$; *y*-axis is parallel to $S_{exo}-Ni-N_{carboxamide}$.

Table 7. Löwdin Orbital Compositions Derived from the DFT Calculations for Selected Molecular Orbitals of Complex **5**

MO label	MO	*E* (eV)	%Ni[a]	%N[b]	%S[c]	orbital composition
LUMO[d]	109	0.64	8.0	19.4	2.3	$Ni(d_{xz}) - N_{py}(p_z), N_{am}(p_z)$
HOMO	108	−0.51	58.4	3.4	26.3	$Ni(d_{yz}) - N_{am}(p_z) - S_{exo}(p_z)$
HOMO-1	107	−0.78	48.0	2.6	31.0	$Ni(d_{xz}) - S_{nmp}(p_z)$
HOMO-2	106	−0.93	93.5	1.7	3.1	$Ni(d_{z2})$
HOMO-3	105	−1.66	48.8	6.5	25.3	$Ni(d_{xy})/Ni(d_{xz}), N_{am}(p_z), S_{exo}(p_z)/S_{exo}(p_x)$
HOMO-4	104	−1.85	29.9	8.4	35.8	$Ni(d_{xy})/Ni(d_{xz}), N_{am}(p_z)/N_{am}(p_y), S_{exo}(p_z)$
HOMO-5	103	−2.10	20.4	5.4	19.5	$Ni(d_{xy})/Ni(d_{xz}), N_{am}(p_x)/N_{am}(p_y)/N_{am}(p_z), S_{nmp}(p_z)/S_{nmp}(p_y)$
HOMO-6	102	−2.30	34.3	1.1	42.4	$Ni(d_{xz})/Ni(d_{yz})/Ni(d_{x2-y2}) + S_{nmp}(p_z), S_{exo}(p_z)$

[a] MO contribution from the Ni AOs. [b] MO contribution from the N AOs of N_{py} and the coordinated $N_{carboxamide}$. [c] MO contribution from the S AOs. The composition is given in order of AO contribution to the MO. [d] The major contributions to the LUMO involves C(pπ) AOs from the pyridine ring of nmp (56.9%). Bonding interactions are represented with a + and antibonding interactions are denoted with a −. The coordinate system used for figuring out the type of AO on Ni, N and S are as follows: *z*-axis is normal to the square planar ligand field; *x*-axis is parallel to $S_{nmp}-Ni-N_{py}$; *y*-axis is parallel to $S_{exo}-Ni-N_{carboxamide}$.

Table 8. Löwdin Orbital Compositions Derived from the DFT Calculations for Selected Molecular Orbitals of Complex **6**

MO label	MO	*E* (eV)	%Ni[a]	%N[b]	%S[c]	orbital composition
LUMO[d]	108	0.69	8.0	19.6	2.4	$Ni(d_{xz}) - N_{py}(p_z), N_{am}(p_z)$
HOMO	107	−0.57	61.2	4.0	22.0	$Ni(d_{yz}) - N_{am}(p_z) - S_{exo}(p_z)$
HOMO-1	106	−0.75	47.0	2.5	32.9	$Ni(d_{xz}), N_{am}(p_z), S_{nmp}(p_z)$
HOMO-2	105	−0.91	93.2	1.6	3.5	$Ni(d_{z2})$
HOMO-3	104	−1.62	50.3	6.1	25.1	$Ni(d_{xy}), N_{am}(p_z), S_{exo}(p_z)/S_{exo}(p_x)$
HOMO-4	103	−1.93	23.1	8.6	31.1	$Ni(d_{xy})/Ni(d_{xz}), N_{am}(p_z)/N_{am}(p_y), S_{exo}(p_z)/S_{exo}(p_y)$
HOMO-5	102	−2.09	24.7	5.6	33.5	$Ni(d_{xy})/Ni(d_{xz}), N_{am}(p_z)/N_{am}(p_x), S_{nmp}(p_z)/S_{nmp}(p_y), S_{exo}(p_z)$
HOMO-6	101	−2.22	34.3	2.6	29.4	$Ni(d_{xz})/Ni(d_{xy})/Ni(_{yz}), N_{am}(p_z)/N_{am}(py)/N_{am}(p_x), S_{nmp}(p_z)$

[a] MO contribution from the Ni AOs. [b] MO contribution from the N AOs of N_{py} and the coordinated $N_{carboxamide}$. [c] MO contribution from the S AOs. The composition is given in order of AO contribution to the MO. [d] The major contributions to the LUMO involves C(pπ) AOs from the pyridine ring of nmp (56.7%). Bonding interactions are represented with a + and antibonding interactions are denoted with a −. The coordinate system used for figuring out the type of AO on Ni, N and S are as follows: *z*-axis is normal to the square planar ligand field; *x*-axis is parallel to $S_{nmp}-Ni-N_{py}$; *y*-axis is parallel to $S_{exo}-Ni-N_{carboxamide}$.

0.64, respectively. ESP maps have been used to rationalize the susceptibility of attack by an electrophile/oxidant;[25] however, they can be computationally expensive without resorting to a point-charge approximation. A simpler approach, which affords a more quantitative comparison, is to compute the ESP analytically at the positions of the nuclei, which has been advocated as a powerful reactivity index by Galabov and co-workers.[99,100] Using this method, we obtain ESPs (in a.u.) at the S_{exo} of −59.4518, −59.4280, and −59.4245 for **3**, **5**, and **6**, respectively (Figure 6, and the Supporting Information, Figure S21). The ~0.03 a.u. difference of the ^{t}BuS-derivative **3** implies stabilization of an oxidizing agent at that S-atom's position by ~0.65 eV or 15 kcal/mol relative to the H-bonded derivatives **5** and **6**. These values are consistent with the electron releasing properties of the ligands, and they accurately correlate the donor strength of the ligand with the nucleophilicity of the S_{exo}-donor. The negative of the HOMO orbital energies of **3**, **5**, and **6** correspond to −0.34 eV, −0.51 eV, and −0.57 eV, respectively (Figure 7, Tables 6−8), and the trend correlates well with the experimentally determined oxidation potentials (vide supra), in keeping with Koopmans' theorem.[101]

The atomic charges on the aryl-S_{exo} of **2** and **4** are −0.18 and −0.26, respectively, (see Supporting Information, Figures S17 and S19) and, as expected, reflect significantly depleted electron density relative to their alkyl congeners. This decrease in electron density is matched by reduced contributions from the S_{exo} to the HOMO,

---

(99) Bobadova-Parvanova, P.; Galabov, B. *J. Phys. Chem. A* **1998**, *102*, 1815.

(100) Galabov, B.; Bobadova-Parvanova, P. *J. Phys. Chem. A* **1999**, *103*, 6793.

(101) Perdew, J. P.; Levy, M. *Phys. Rev. B* **1997**, *56*, 16021.

with S_{exo} of **2** and **4** contributing only 0.5% (40.3% total S) and 0.4% (41.8% total S), respectively. In contrast to **3**, **5**, and **6**, the differences between the Ni contributions to the HOMO arising from **2** and **4** vary much less, ranging from 42.3% to 41.3% for **2** and **4**, respectively. The HOMO energies tend to be lower than those in the alkyl S_{exo} systems, which possess less contracted lone pairs on S, consistent with the conjecture that repulsive $d(\pi)$-$p(\pi)$ interactions between Ni and S raise the energy of the HOMO.[25,27,28,30] As before, the experimental oxidation potentials of **2** and **4** match the relative trends in the negative of the HOMO energies which are found to be −0.73 eV and −0.88 eV, respectively.

Previous computational studies suggest that the effects of protonation or H-bonding to coordinated thiolates impart profound effects on the electronic structures of some analogous NiN_2S_2−SOD model systems.[25,30] Our results reveal that the atomic charges on the thiolato-S of **2**−**6** do not reflect the presence of the H-bond; as the atomic charges on the S-atoms of **3**, **5** and **6** are relatively invariant. These values are rather unexpected, given that H-bonding is expected to deplete the electron density at S. Thus, H-bonding does not appear to shift charge away from S to a significant extent, however, evidence of charge neutralization at S is reflected in the more positive ESP. Even though charge density is polarized away from a particular nucleus it is still assigned to the same atom if it is closest to that nucleus. Therefore, the positive induced dipole is not reflected in charge if polarization is small, as in H-bonding. Notwithstanding the fact that ligand donor strength also plays a role, we can see that the ESPs of the monodentate thiolate ligands of **5** and **6**, which possess intramolecular H-bonds, are lower than that of **3** (Figure 6, and the Supporting Information, Figure S21). The same effect is observed for the monodentate thiolate of **4**, which possesses a lower ESP than that of **2** (see the Supporting Information). Thus, it appears that H-bonding to coordinated thiolates is manifested in a decreased ESP, and not the atomic charges. *This effect, coupled with the decrease in thiolato-S contribution to the HOMO and concurrent increase in that arising from Ni, strongly suggests that H-bonding to Ni-bound thiolates results in a reduced propensity for ligand-based oxidation.* Taken together, the presence of intramolecular H-bonds in Ni-SOD may, *in combination* with the unique set of N-donor ligands present, provide a means of protecting the coordinated Cys-S donors during catalysis.

Conclusions

In summary, we have prepared and extensively characterized five $Ni^{II}N_2S_2$ complexes of the general formula $[Ni^{II}(nmp)(SR)]^-$, which conform nicely as structural biomimetics of the Ni-SOD_{red} active site. Complexes **2**−**6** were constructed via three chemically distinct synthetic procedures: (i) direct S,S-bridge splitting of dimer **1**; (ii) a disulfide/coordinated thiolate exchange reaction via the addition of 0.5 mol-equiv of a weaker S_{exo}-donor in its disulfide form; and (iii) thiol/coordinated thiolate exchange through addition of 1 mol-equiv of a less basic S_{exo}-donor in its thiol form. These methodologies provide a facile means to incorporate thiolate ligands of variant donor strength and, in the present account, to introduce secondary sphere interactions such as H-bonding. These ligand variations, along with other types of modifications, have opened up an expansive library of complexes built off of one common metallosynthon, namely, the Ni(nmp) fragment. This approach provides a unique opportunity to probe the role played by the cysteine thiolates and the influence of the immediate chemical environment in Ni-SOD, and by analogy, other biomolecules employing Ni-thiolate coordination.[21,22]

The existence of intramolecular NH···S bonding in the solution-state of complexes **4**−**6** was corroborated by the large downfield chemical shifts observed in the ^{1}H NMR and the red-shifts in ν_{NH} and ν_{CO} in the FTIR spectra compared to those of the disulfide or thiol form of the variable S_{exo} ligand. The intramolecular H-bond is also visible in the X-ray structure of **4**, resulting in a ~0.03 Å contraction of the Ni−S_{exo} bond. Electrochemical measurements revealed significant cathodic shifts in the H-bonded complexes by 40 mV in the aryl systems **2** and **4** and ~150−200 mV among the alkyl systems **3**, **5**, and **6**. By separately analyzing the complexes featuring aryl- and alkyl-S_{exo} ligands, it becomes clear that the oxidation potentials of the $Ni^{II}N_2S_2$ complexes increase as the donor strength of S_{exo} decreases. Analysis of the trends observed suggests that H-bonding to coordinated thiolates plays a significant role in modulating these potentials much like what has been observed in other synthetic analogue systems.[72]

Complexes **2**−**6** were shown to react with ROS and $O_2(g)$, revealing for the first time, quantitative kinetic information regarding the oxidative stability of Ni-SOD_{red} models. Reaction with $O_2(g)$ under pseudo first-order conditions is a relatively slow process and afforded selective S_{exo} modification at rates on the order of 10^{-5}−10^{-4} s^{-1} in MeCN at 298 K. Reactions with excess H_2O_2 under similar conditions were less discriminate, affording mixtures of species and a rate of decay (10^{-2} s^{-1}) that was several orders of magnitude faster than reaction with $O_2(g)$, although a ~ 6-fold decrease in k_{obs} was noted for the H-bonded systems **5** and **6**, suggestive of some degree of protection from the H-bonds. Furthermore, addition of excess $O_2^{\bullet-}$ effects no defined changes in the UV spectra (in MeCN) of the complexes and thus does not disproportionate $O_2^{\bullet-}$ under these conditions even in the presence of a potential axial N-donor. These results have provided initial insight into the reactivity trends observed via manipulation of the S_{exo} appended to the Ni(nmp) framework and into how this effect translates into oxidative stability of the Ni-SOD active site.

DFT optimized models of **2**−**6** were generated and reflect those determined experimentally by crystallography. The effect of H-bond incorporation is clearly demonstrated in the frontier MOs of the Ni^{II} complexes. In the alkyl-S_{exo} systems, H-bonding serves to stabilize both the LUMO and HOMO by ~0.30 and 0.20 eV, respectively. Additionally, H-bonding results in significantly more Ni- and less S-character in the HOMO and low-lying HOMO-1 of **5** and **6** compared to the non-H-bonded complex **3**. ESP calculations of the H-bonded S_{exo} in **5** and **6** also reveal a 15 kcal/mol stabilization against oxidants with respect to **3**. Thus, H-bonding to coordinated thiolates reveals multiple degrees of systemic changes reflected in the solid-state structures, redox potentials, spectroscopic properties, and electronics. These observations advocate an approach whereby the H-bonded cysteine thiolates found in the Ni-SOD active site may be protected from oxidative modification. This degree of protection may be more significant in Ni-SOD$_{red}$ as the principle bonding interactions are defined by the highly covalent nature of the π-based HOMO and HOMO-1, containing a large amount of both Ni- and CysS-character.[30] Upon coordination of the His1 N$_{Im}$ in Ni-SOD$_{ox}$, the MOs rearrange to define a principally Ni-based (d_{z^2}) σ-bonding feature in the HOMO.[30] The different character in Ni-SOD$_{ox}$ provides the rationale for Ni- versus S-based redox chemistry in this state of the enzyme, since no significant S-character is observed in the HOMO. Site-directed mutagenesis studies confirm the necessity of this bond[102] and some suggest that the Ni$-$N$_{His1}$ bond remains throughout catalysis.[32] Obviously, this interaction is presently absent in our models systems; however, efforts are underway to further elucidate this crucial interaction in our laboratory.

Acknowledgment. T.C.H. acknowledges support from an NSF CAREER Award (CHE-0953102), the Department of Chemistry at the University of Georgia (UGA) for startup funds, and the UGA Research Foundation (UGARF) for a faculty research award. H.F.S. acknowledges support from the NSF (CHE-0749868). We wish to thank Franklin E. Leach III and Prof. I. Jonathan Amster for assistance with the high resolution ESI-MS measurements. We also wish to thank Dr. Ashis K. Patra for assistance with X-ray crystallography.

Note Added after ASAP Publication. This paper was published on the Web on June 24, 2010, with a misspelled authors name in ref 8 and a minor text error at the end of the second paragraph on page 13 of the paper. The corrected version was reposted on June 29, 2010.

Supporting Information Available: X-ray crystallographic data including CIF files, high-resolution ESI-MS of **6**, computational results including Cartesian coordinates, optimized geometries, and MO diagrams of **2** and **4**, UV$-$vis and ESI-MS results of the $O_2(g)$, H_2O_2, and superoxide studies and complete reference 68. This material is available free of charge via the Internet at http://pubs.acs.org.

---

(102) Bryngelson, P. A.; Arobo, S. E.; Pinkham, J. L.; Cabelli, D. E.; Maroney, M. J. *J. Am. Chem. Soc.* **2004**, *126*, 460.